iScience

CellPress
OPEN ACCESS

Article

Trichinella spiralis inhibits myoblast differentiation by targeting SQSTM1/p62 with a secreted E3 ubiquitin ligase

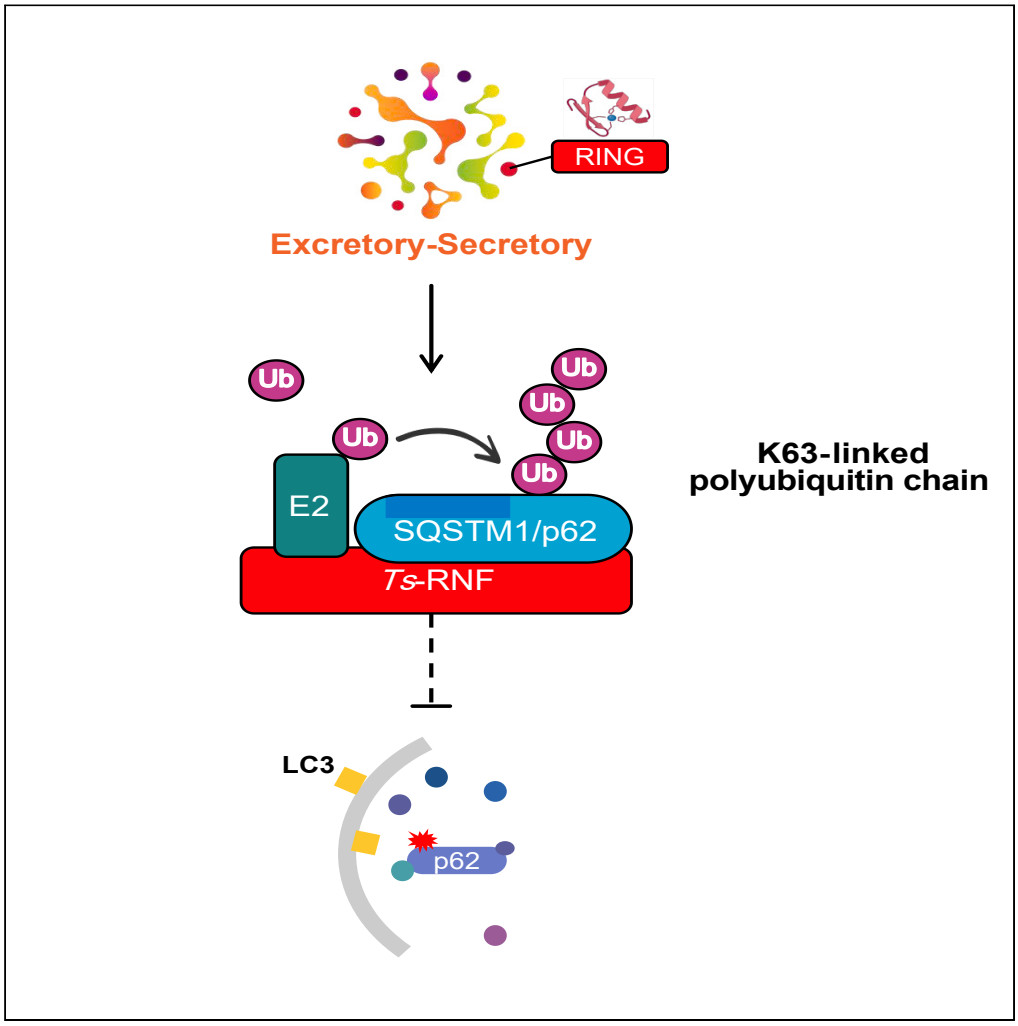

Jian da Pang, Xue min Jin, Yi Liu, ..., Ming yuan Liu, Ning Xu, Xiao lei Liu

beyond44141@163.com (N.X.)
liuxlei@163.com (X.l.L.)

Highlights

Trichinella spiralis-secreted *Ts*-RNF exhibits E3 ubiquitin ligase activity

Interaction of *Ts*-RNF with SQSTM1/P62 UBA domain

Interfering with the *Ts*-RNF gene can hinder the growth and development of *T. spiralis*

Ts-RNF hinders mitochondrial clearance and affects muscle differentiation

Pang et al., iScience *27*, 109102
March 15, 2024
https://doi.org/10.1016/j.isci.2024.109102

iScience

CellPress
OPEN ACCESS

Article

Trichinella spiralis inhibits myoblast differentiation by targeting SQSTM1/p62 with a secreted E3 ubiquitin ligase

Jian da Pang,[1,4] Xue min Jin,[1,4] Yi Liu,[1,4] Zi jian Dong,[1] Jing Ding,[1] Pascal Boireau,[3] Isabelle Vallée,[3] Ming yuan Liu,[1,2] Ning Xu,[1,*] and Xiao lei Liu[1,5,*]

SUMMARY

Trichinella spiralis infection is associated with the formation of cysts within host skeletal muscle cells, thereby enabling immune evasion and subsequent growth and development; however, the pathogenic factors involved in this process and their mechanisms remain elusive. Here, we found that _Ts_-RNF secreted by _T. spiralis_ is required for its growth and development in host cells. Further study revealed that _Ts_-RNF functions as an E3 ubiquitin ligase that targets the UBA domain of SQSTM1/p62 by forming K63-type ubiquitin chains. This modification interferes with autophagic flux, leading to impaired mitochondrial clearance and abnormal myotube differentiation and fusion. Our results established that _T. spiralis_ increases its escape by interfering with host autophagy via the secretion of an E3 ubiquitin ligase.

INTRODUCTION

Trichinella spiralis is a significant zoonotic pathogen with a complex life cycle, and severe infections can result in host mortality. Newborn larvae (NBL) migrate through the blood and lymphatic vessels to skeletal muscle cells.[1] After a newborn larva has entered the host muscle cells, satellite cells are activated and begin to proliferate. However, this process inhibits differentiation and alters normal muscle repair processes, thereby leading to the formation of a highly vascularized collagen-surrounded cyst that nourishes and shields the parasite from host immune responses.[2,3] This process also causes mitochondrial damage and dysfunction.[4] Previous research has shown that *T. spiralis* muscle larvae excretory-secretory products (ML-ES) can effectively promote myoblast proliferation and inhibit myoblast differentiation.[5,6] Additionally, we found that autophagy is regulated during *T. spiralis* infection, and ML-ES leads to hindered myoblast differentiation by influencing the MAPK signaling pathway.[7] This indicates that critical mediators present in ML-ES have an inhibitory effect on myoblast differentiation. However, the intricate pathways and molecular mechanisms involved in cyst formation are still unclear.

T. spiralis invades skeletal muscle cells to form tissue cysts, leading to a significant decline in muscle function and delayed repair. This phenomenon is also commonly observed in aging and degenerative diseases. The disruption of protein homeostasis, which is closely associated with the ubiquitin-proteasome pathway, mainly contributes to this phenomenon. Protein ubiquitination is a reversible posttranslational modification that is critical for many cellular processes.[8] Ubiquitin can be linked to seven lysine (K) residues or the N-terminus of another ubiquitin and form polyubiquitin chains with complex topologies.[9] Ubiquitination requires the transfer of ubiquitin from the ubiquitin-activating enzyme E1 to an E2-conjugating enzyme. E3 ubiquitin ligases covalently modify protein substrates by catalyzing ubiquitin transfer from an E2-conjugating enzyme to substrate proteins.[10] Many viral and bacterial E3 ligases have been identified and some exhibit protein sequence homology and target host defense proteins for degradation or modification.[11] *Shigella flexneri*,[12] *Salmonella typhimurium*,[13] *Legionella pneumophila*,[14] and other pathogens employ diverse E3 ligases, such as secreted effector proteins and toxins. These pathogens exploit the host ubiquitin system to evade defenses.[15,16]

Parasites secrete highly complex products containing hundreds of proteins, carbohydrates, lipids, nucleotides, and vesicles. Each protein might act at different phases of infection to modulate the host immune response.[17] Recent research on parasites has focused on elucidating the crucial or indispensable components of the endogenous Ub system that are pivotal for parasite biology. A *Toxoplasma cruzi* secreted protein with a RING-domain-exhibited E3 ligase activity and was localized in the host nucleus.[18] The *Plasmodium yoelii* gene encodes an HECT-like E3 ubiquitin ligase (*Pyheul*) that affects parasitemia and host mortality.[19] An investigation of *T. spiralis*-specific enzymes revealed that the E2-conjugating enzyme *Ts*UBE2L3 in ML-ES has the capability to interact with host proteins and influence muscle protein expression.[20]

[1]State Key Laboratory for Diagnosis and Treatment of Severe Zoonotic Infectious Diseases, Key Laboratory for Zoonosis Research of the Ministry of Education, Institute of Zoonosis, College of Veterinary Medicine, Jilin University, Changchun, Jilin 130062, China
[2]Jiangsu Co-innovation Center for Prevention and Control of Important Animal Infectious Diseases and Zoonoses, Yangzhou, Jiangsu 225000, China
[3]Ecole Nationale Vétérinaire d'Alfort, Laboratoire de Santé Animale, BIPAR, 94700 Maisons-Alfort, France
[4]These authors contributed equally
[5]Lead contact
*Correspondence: beyond44141@163.com (N.X.), liuxlei@163.com (X.l.L.)
https://doi.org/10.1016/j.isci.2024.109102

This early research demonstrated that the ubiquitination pathway represents a feasible strategy for promoting *T. spiralis* infection. Although the presence of parasite ubiquitination enzymes has been established in prior studies, the functional role and specific mechanism of these enzymes in parasite invasion have largely not been unexplored.

In our previous transcriptome analysis of *T. spiralis* and *Trichinella pseudospiralis*, we identified a significantly differentially expressed gene belonging to the RING-Ubox superfamily that was annotated as RNF-type ubiquitin ligase (GenBank: KRY41185) in the *T. spiralis* gene bank. Structural modeling revealed that *Ts*-RNF exhibits similarities with the E3 ubiquitin ligases RNF128, RNF38, and RNF13.[21] In this study, we demonstrated that *Ts*-RNF functions as an E3 ubiquitin ligase and identified the modification sites of its substrate through quantitative-ubiquitination-modified proteomics. We observed that *Ts*-RNF interacts with host p62 and mediates K63-linked ubiquitination of the UBA domain at residue K422. *Ts*-RNF interferes with the host ubiquitination pathway and selective autophagy pathways, thereby impairing mitochondrial clearance during myoblast differentiation and abnormal myotube differentiation and fusion. These findings provide insights into *T. spiralis* cyst formation mechanisms and potential new therapeutic targets for trichinosis.

RESULTS

T. spiralis-secreted *Ts*-RNF has E3 ubiquitin ligase activity

An *in vitro* Ub conjugation assay was conducted to determine whether ES from *T. spiralis* muscle larvae had E2 or E3 enzymatic activity. As a positive control, a reaction was conducted with Ub-HA, E1 (UBE1), E2 (UBE2L3), E3 (parkin), and the substrate His-S5a. The presence of parkin resulted in the ubiquitination of the substrate, which was observed as an anti-HA smear. ML-ES was then substituted into the reaction for either E2 or E3. When E2 (UBE2L3) or E3 (parkin) was replaced with ML-ES proteins, a ubiquitination signal representing ES was also observed. When E3 was removed from the reaction, no signal was observed. This suggests that ML-ES has E2 and E3 activity (Figures 1A and S2). To further confirm whether *Ts*-RNF has E3 ubiquitin ligase activity, we performed an *in vitro* ubiquitination experiment.[20] The coupled reticulocyte lysate systems were utilized to conduct reactions for eukaryotic *in vitro* translation.[22] In this way, the *Ts*-RNF soluble protein was obtained for the activity assay.[22] The Ub signal was observed when *Ts*-RNF was substituted in the place of parkin. When E3 was removed from the reaction, no signal was observed. These findings indicate that *Ts*-RNF has E3 ligase activity (Figure 1B). The recombinant protein r*Ts*-RNF was expressed via a prokaryotic expression system. Polyclonal anti-*Ts*-RNF (*Ts*-RNF Rb pAb) was obtained from rabbits immunized with purified recombinant r*Ts*-RNF protein. *Ts-RNF* protein was not detected in the skeletal muscles of uninfected mice, but it was found in *T. spiralis* and ES. These results showed that *Ts*-RNF is a secreted protein (Figure 1C). Moreover, quantitative analysis also revealed that *Ts*-RNF mRNA expression was highest in the ML and adult (AD) stages (Figure 1D). The *Ts*-RNF and ubiquitination in *T. spiralis*-infected skeletal muscle were detected using an immunofluorescence double-labeling method. For negative controls, primary antibodies were replaced with preimmune serum and PBS. The staining results indicated that *Ts*-RNF was primarily expressed on the surface of the helminth and within the cyst. A high level of ubiquitin was also observed in infected skeletal muscle (Figure 1E).

Ts-RNF causes abnormal differentiation of myoblasts

The C2C12 cell line is a mouse myoblast line that is widely used as an *in vitro* model of skeletal muscle cell biology. The differentiation of C2C12 myoblasts into myotubes represents a mature model of muscle cell differentiation.[23,24] The lentiviral overexpression vector *Ts*-RNF was used to infect C2C12 cells, and the empty lentiviral vector served as the negative control (NC). Stable *Ts*-RNF-transfected cell lines were established through puromycin screening for subsequent experiments. Western blotting demonstrated that *Ts*-RNF can be stably expressed at various stages of differentiation (Figure S3). The results of tubulin protein immunofluorescence staining revealed apparent aberrant differentiation in the *Ts*-RNF group compared with the NC group on day 8 of differentiation (Figure 2A). Myotube heavy chain (MyHC) immunofluorescence intensity was also assessed, as MyHC protein expression is a hallmark of myotube formation. The results showed that *Ts*-RNF overexpression reduced the formation of myotubes in the *Ts*-RNF groups compared with the control group, and there were undifferentiated cells (Figure 2B). Subsequently, we studied the effects of *Ts*-RNF on C2C12 cell proliferation and cell-cycle progression. The impact on cell viability and proliferation was evaluated using the CCK8 assay for cell viability and the Ki67 marker for proliferation. These results showed that *Ts*-RNF reduced cell viability and inhibited cell proliferation in C2C12 cells (Figure 2C). Flow cytometry analysis of the cell cycle showed that the proportion of cells in the G1 phase was greater in the *Ts*-RNF group than in the NC group and normal group during the initial differentiation stage (Figure S4A). We next determined the degree of protein ubiquitination at different time points during myoblast differentiation. Western blotting analysis revealed greater ubiquitination levels in the *Ts*-RNF group than in the NC group (Figure 2D). Finally, we analyzed the protein expression and mRNA expression of the myogenic markers MyHC, MyoD, and MyoG at various stages of differentiation. The expression levels of these protein markers in the NC group were higher than those in the *Ts*-RNF group at three different time points (Figure 2E). The mRNA expression levels in the NC group were significantly higher than those in the *Ts*-RNF group on day 4 and day 8 of differentiation (Figure S4B). We also examined the expression levels of the fusion markers Myomarker and Myomixer. It was evident that *Ts*-RNF inhibited both terminal differentiation and cell fusion (Figure 2F). These findings suggest that *Ts*-RNF not only inhibits both myoblast proliferation and differentiation but also leads to the aberrant fusion of myotubes.

Ts-RNF was shown to interact with SQSTM1/p62 by quantitative-ubiquitination-modified proteomics

To elucidate the mechanism by which *Ts*-RNF inhibits C2C12 cell differentiation, we screened for *Ts*-RNF-interacting substrates and identified ubiquitination sites. *Ts*-RNF group cells were treated with 20 μM of the proteasome inhibitor MG132 for 6 h to suppress *Ts*-RNF-dependent

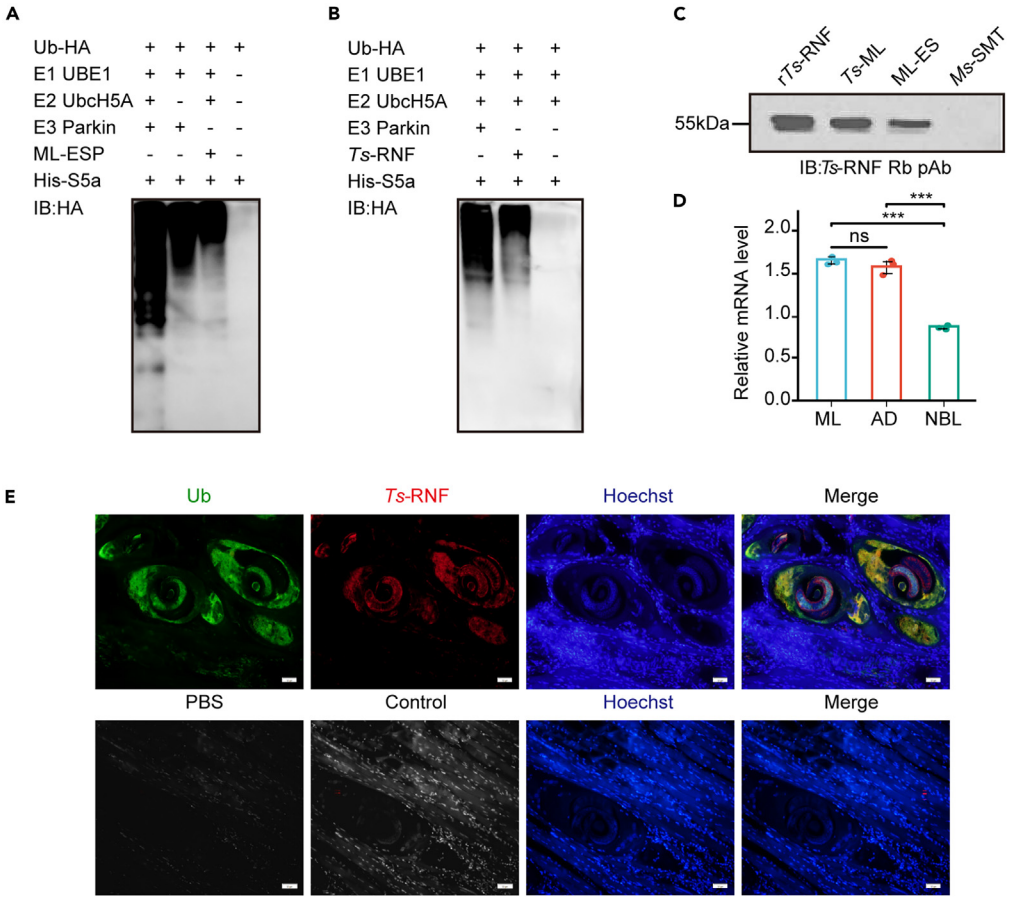

Figure 1. *Trichinella spiralis*-secreted *Ts*-RNF has E3 ubiquitin ligase activity

(A) *In vitro* ubiquitination assay showing the E2 ubiquitin-conjugating enzyme and E3 ubiquitin ligase activity of muscle larvae excretory-secretory products (ML-ES); ML-ES was incubated with HA-Ub, E1 (UBE1), HisS5a, and ATP buffer at 37°C for 2 h in the presence or absence of E2 (UbcH5A) or E3 (Parkin). After the termination, the reaction mixture was subjected to SDS-PAGE and immunoblotting assay with an anti-HA antibody.

(B) *In vitro* ubiquitination assay showing the E3 ubiquitin ligase activity of *Ts*-RNF. The *Ts*-RNF protein was incubated with HA-Ub, E1 (UBE1), E2 (UbcH5A), HisS5a, and ATP buffer in the presence or absence of the E3 (Parkin) protein at 37°C for 2 h. After the termination, the reaction mixture was subjected to SDS-PAGE and immunoblotting assay with an anti-HA antibody.

(C) *Ts*-RNF-specific antibody was made and its specificity was assessed by immunoblotting against muscle larvae lysate (*Ts*-ML), ML-ES, and uninfected skeletal muscle tissue lysate (SMT).

(D) Expression analysis of *Ts*-RNF at different developmental stages (n = 3). ML, muscle larvae; AD, adults; NBL, newborn larvae. Data are shown as the means ± SEMs from three independent experiments. Statistical analysis was performed using one-way ANOVA test. *$p < 0.05$, **$p < 0.01$, ***$p < 0.001$; ns, not significant.

(E) Confocal microscopy analysis demonstrating colocalization of ubiquitin (green), *Ts*-RNF (red), and Hoechst (blue) in the skeletal muscle of mice infected with *T. spiralis*. For the Ub negative control, PBS was used to replace the primary antibody, and for the *Ts*-RNF negative control, the primary antibody was replaced with preimmune serum. Representative single optical sections and merged images are shown. Scale bars: 50 μm.

ubiquitination. Label-free quantitative proteomics and ubiquitination-modified proteomics analyses were performed on samples from the NC group, the *Ts*-RNF group, and the *Ts*-RNF+MG132 group on day 8 of differentiation (Figure 3A). A total of 22,625 peptides were discovered via protein extraction, enzyme digestion, modified peptide enrichment, liquid chromatography-tandem mass spectrometry (LC-MS/MS) analysis, and bioinformatics analysis (Figures 3B and S5A). Next, we performed a cluster analysis of the differentially expressed proteins. The identified proteins were primarily involved in various biological processes including muscle development and contraction, organelle fusion, protein anabolism, and lipid metabolism. In terms of cellular components, these differentially expressed proteins predominantly resided were enriched in secretory vesicles, proteasomes, ribosomes, and other membrane-related components. These proteins exhibited significant enrichment in molecular functions associated with the actin cytoskeleton, the ubiquitin-proteasome pathway, ribosome-associated enzymes, and other functions (Figure S5B).

We next performed co-IP experiments, followed by mass spectrometric analysis to identify interacting proteins (Figure 3C).[25,26] Cell lysates and anti-FLAG beads samples were separated by SDS-PAGE on day 8 of differentiation. A total of 207 and 213 proteins were identified in the *Ts*-RNF and *Ts*-RNF+MG132 groups, respectively (Figures 3C and S5C). The analysis of the *Ts*-RNF and *Ts*-RNF+MG132 group substrate

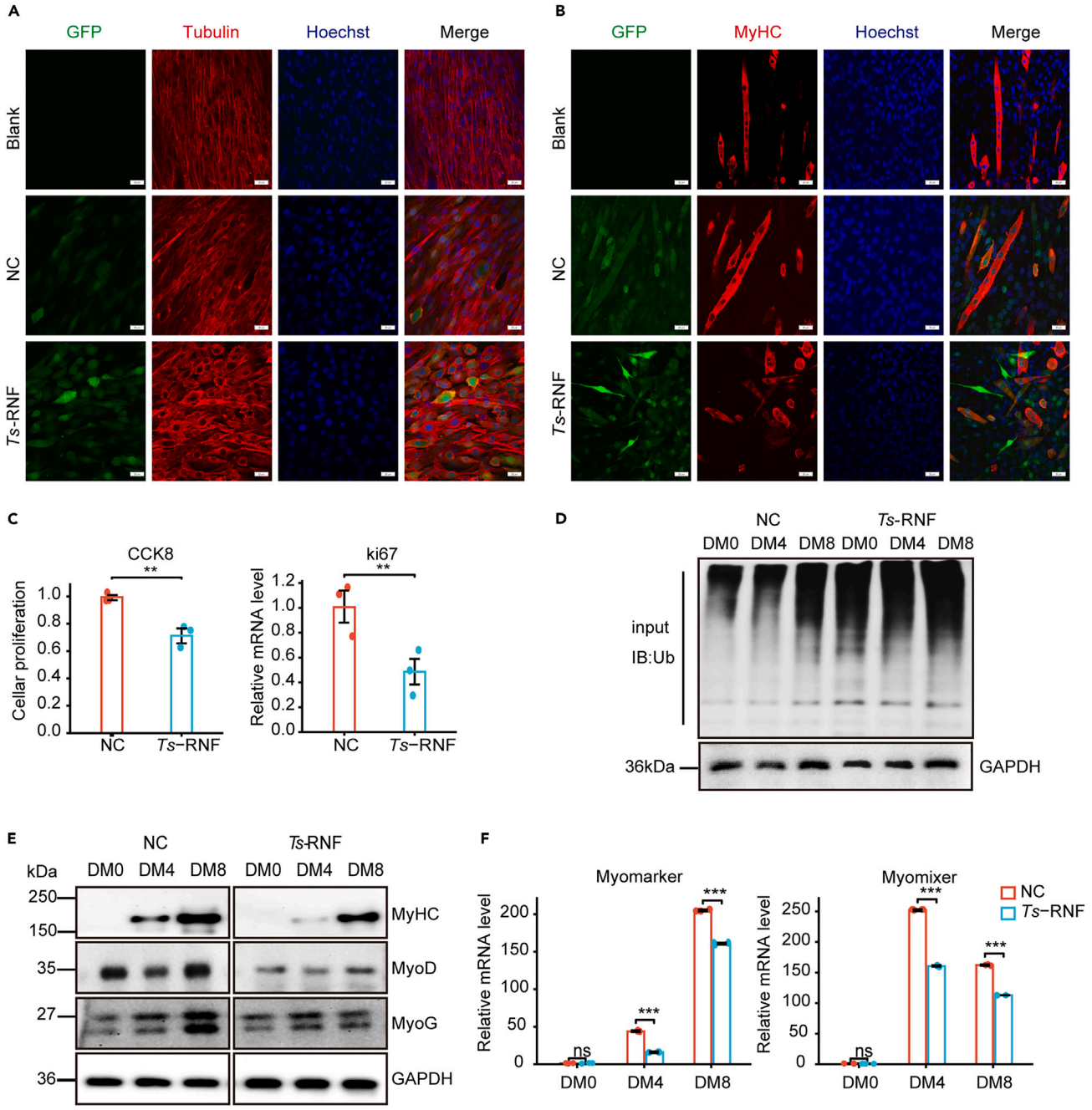

Figure 2. *Ts*-RNF causes abnormal differentiation of myoblasts

(A and B) Confocal microscopy images of tubulin and myotube heavy chain (MyHC) in myotubes eight days after initiation of differentiation. *Ts*-RNF (green), MyHC (red), and Hoechst (blue). Cells were transfected with a plasmid with gene encoding the *Ts*-RNF gene. Untransfected cells (Blank) and cells transfected with empty vector served as negative controls (NC). Representative single optical sections and merged images are shown. Scale bars: 20 μm.

(C) The CCK-8 assay was used to analyze the viability of *Ts*-RNF- and NC-transfected cells. The expression levels of the Ki67 gene in the NC group and *Ts*-RNF group were quantitatively analyzed in undifferentiated C2C12 cells. Data are shown as the means ± SEMs from three independent experiments (n = 3). Statistical analysis was performed using independent samples t test. *$p < 0.05$, **$p < 0.01$, ***$p < 0.001$; ns, not significant.

(D) The ubiquitination level of myoblast differentiation was analyzed at different time points in the NC and *Ts*-RNF groups using an *in vitro* ubiquitination assay (DM differentiation medium).

(E) Representative immunoblots of differentiation markers (MyoD, MyoG, MyHC) at different time points in the NC and *Ts*-RNF groups.

(F) The mRNA expression levels of the fusion markers (Myomarker and Myomixer) at different time points in the NC group and *Ts*-RNF group. Data are shown as the means ± SEMs from three independent experiments (n = 3). Statistical analysis was performed using Mann-Whitney U test. *$p < 0.05$, **$p < 0.01$, ***$p < 0.001$; ns, not significant.

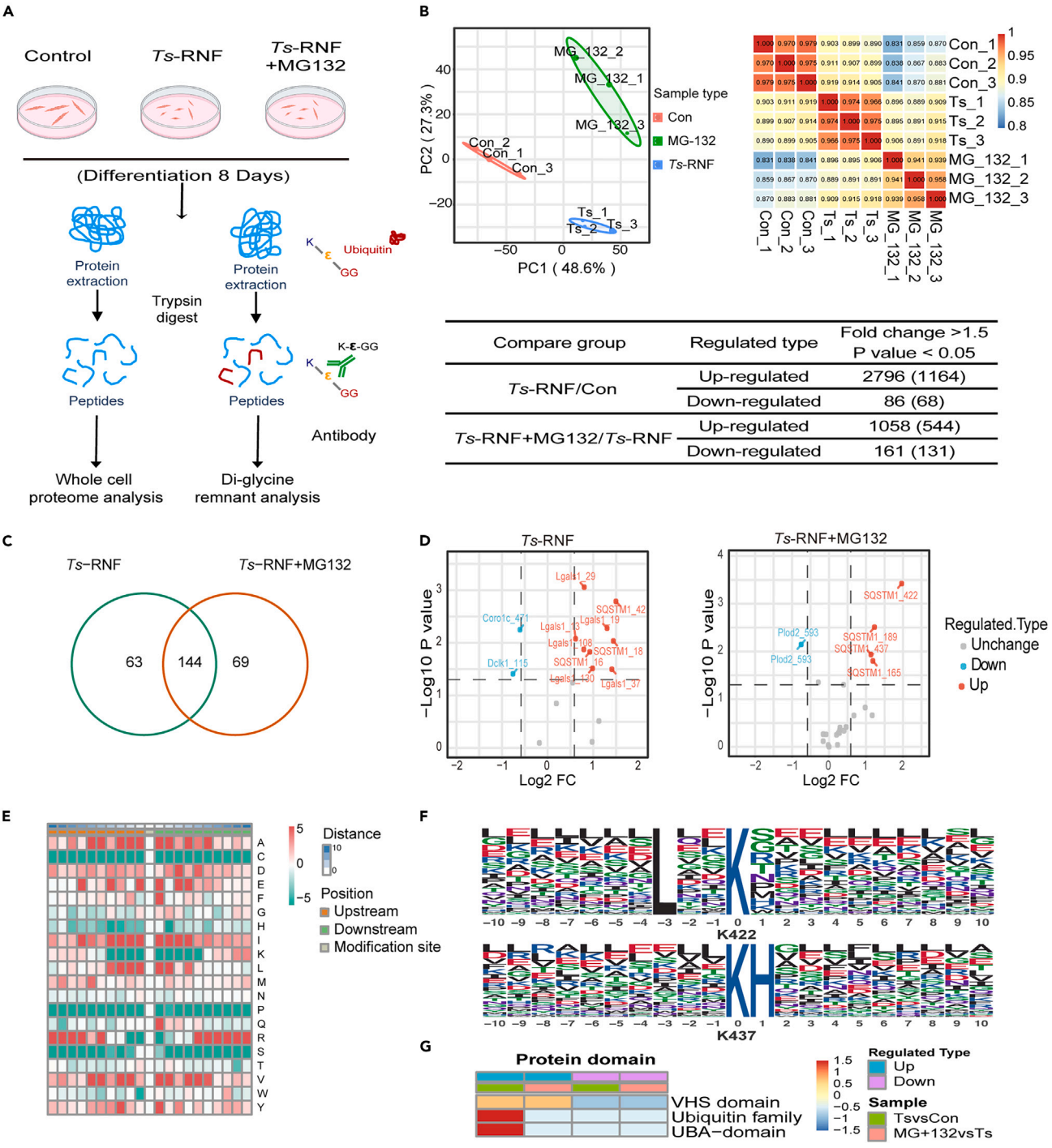

Compare group	Regulated type	Fold change >1.5 P value < 0.05
Ts-RNF/Con	Up-regulated	2796 (1164)
	Down-regulated	86 (68)
Ts-RNF+MG132/*Ts*-RNF	Up-regulated	1058 (544)
	Down-regulated	161 (131)

Figure 3. *Ts*-RNF can interact with SQSTM1/p62, as shown by quantitative proteomic screening with ubiquitination

(A) Illustration of the workflow for quantitative-ubiquitination-modified proteomics.

(B) Principal-component analysis (PCA) scatterplots reveal protein expression in each sample, and Pearson correlation analysis generates heatmaps of quantified protein expression. A summary table provides quantitative-ubiquitination-modified proteomic results.

(C) The cell lysates were immunoprecipitated with anti-Flag beads and then analyzed by mass spectrometry. Venn diagram summarizing the obtained screening results from co-IP substrate protein screening for two independent experiments. Supplemental data related to this Figure are shown in Table S2.

(D) Protein modification of *Ts*-RNF substrate differentially expressed (orange represents upregulation, blue downregulation, and gray indicates no relevant difference).

Figure 3. *Continued*

(E) Heatmap of amino acid enrichment upstream and downstream of *Ts*-RNF substrate differentially ubiquitinated conjugation sites (10 residues each upstream and downstream). The center column corresponds to the ubiquitinated lysine (A–Y). High frequency is indicated by red and low frequency by green. Supplemental data related to this Figure are shown in Table S3.

(F) Motif feature map of the p62 ubiquitination sites (K422 and K437 are highly scaled to reflect motif features).

(G) The significantly enriched protein domains of differentially identified substrates (red indicates strong enrichment, and blue indicates weak enrichment).

proteomic data showed that the Lgals1 and SQSTM1/p62 proteins were specifically increased in the *Ts*-RNF group, whereas the Dclk1 and Coro1c proteins were specifically decreased. Additionally, SQSTM1/p62 expression was upregulated and Plod2 expression was downregulated in the *Ts*-RNF+MG132 group (Figures 3D and S5D). The multifunctional adaptor protein SQSTM1/p62 is implicated in selective autophagy and plays a crucial role in regulating multiple cellular functions through its diverse domains that facilitate interactions with various signaling proteins. Motif analysis of the differentially expressed substrate protein modification sites revealed that the significantly different protein modification sites were K422 and K437 of SQSTM1/p62 (Figures 3E and 3F). Next, analysis of the enriched differentially expressed substrate protein domains revealed predominant enrichment of the ubiquitin family and ubiquitin-associated (UBA) domain in both the *Ts*-RNF vs. Con group (Figure 3G). In summary, quantitative-ubiquitination-modified proteomics and co-IP experiments demonstrated that *Ts*-RNF inhibits C2C12 cell differentiation by directly regulating autophagy-related proteins or pathways.

Ts-RNF interacts with SQSTM1/p62 K422 via K63-linked ubiquitin chains

To verify the interaction between *Ts*-RNF and p62, we constructed expression vectors for Flag-*Ts*-RNF, Myc-p62, and Myc-p62mutants. These vectors were cotransfected into HEK293T cells, which were subsequently lysed and subjected to coimmunoprecipitation experiments using anti-Flag antibody beads. The immunoprecipitates were analyzed by western blotting using anti-Myc antibodies. Co-IP and western blotting revealed that deletion of the UBA domain (Myc-p62 $\triangle$ 334–434) decreased the interaction with *Ts*-RNF, indicating that the UBA domain of p62 is necessary for this interaction (Figure 4A and S6A). In our proteomic modification study, we identified two ubiquitination sites in the UBA domain. We constructed a mutant form of p62 with mutations at positions K422 and K437 of the UBA domain (Figure S6B). Interactions with *Ts*-RNF and p62 were almost undetectable at the K422 mutation site (Figure 4B). This result fully validates the differences found in the proteomic analyses. We next used a reciprocal series of Ub mutants. HA-Ub K-only mutants denote that the only lysine in the HA-tagged ubiquitin is at the indicated residue, and all other lysine residues are mutated to arginine. HA-Ub mutants were cotransfected with Flag-*Ts*-RNF and Myc-p62 into HEK293T cells (Figure S6C). Coimmunoprecipitation analyses revealed that the Myc-p62 mutant was still ubiquitinated in the presence of K63-only ubiquitin, suggesting that *Ts*-RNF may primarily mediate K63-linked ubiquitination of p62 (Figure 4C). Moreover, an *in vitro* ubiquitination assay revealed that the *Ts*-RNF protein could directly add ubiquitin-charged E1and E2 to the p62 protein, suggesting that *Ts*-RNF is an E3 ligase that mediates the ubiquitination of p62 (Figure 4D). *In vitro* ubiquitination assays with recombinant ubiquitin-WT, ubiquitin-K63, and ubiquitin-K63R showed that p62 ubiquitination was induced in the presence of E1, E2, and *Ts*-RNF together with ubiquitin-WT or ubiquitin-K63 but not ubiquitin-K63R. The results indicated that *Ts*-RNF can conjugate poly-Ub chains onto p62 via K63-linkages *in vitro* (Figure 4E). Taken together, our *in vivo* and *in vitro* studies indicate that *Ts*-RNF mediates K63-linked ubiquitination of p62 via the UBA domain.

Ts-RNF interacted with SQSTM1/p62 to mediate mitochondrial clearance in C2C12 cells

To confirm the significance of the *Ts*-RNF and p62 interaction and explore the effect of the *Ts*-RNF and p62 interaction on C2C12 cell differentiation, the effects of *Ts*-RNF on the endogenous expression levels of p62 were analyzed by immunofluorescence staining on day 8 of differentiation. We found that the accumulation of p62 increased in the *Ts*-RNF group during aberrant differentiation (Figure 5A). Western blotting results revealed an upregulation of Pink1 and Parkin expression levels in the *Ts*-RNF group compared with the NC group at various time points following differentiation. In contrast to those in the control group, the autophagic flux in the *Ts*-RNF group exhibited a deficiency during the initial stages of C2C12 differentiation, with reduced expression of LC3-II and accumulation of p62 observed at the end of differentiation in contrast to the control group (Figures 5B and S7A). We also examined the mitochondrial membrane potential using the fluorescent probe of tetramethylrhodamine ethyl ester (TMRE). As a control, cells were treated with the protonophore carbonyl cyanide p-trifluoromethoxy-phenylhydrazone (CCCP) to induce the loss of mitochondrial membrane potential, which strongly decreased TMRE fluorescence. On day 8 of differentiation, *Ts*-RNF also led to a decrease in the mitochondrial membrane potential (Figure 5C). Normal differentiated cells were treated with SOD (superoxide dismutase) as a positive control, and superoxide production was measured using a superoxide anion detection kit. The measured OD values demonstrated a significantly elevated level of superoxide anions in the *Ts*-RNF group compared with both the NC group and the SOD-treated group (Figure 5D). Ultrastructural changes in mitochondria and autolysosomes were evaluated using transmission electron microscopy (TEM) on day 8 of differentiation. TEM analysis revealed normal mitochondrial morphology and typical autolysosomes in both normal cells and the NC group. However, the *Ts*-RNF group exhibited mitochondrial and autolysosome morphology defects, loss of membrane integrity, and an increased number of lipid droplets on the eighth day of differentiation (Figure 5E). Quantitative analysis of the gene expression of the inflammatory factors tumor necrosis factor alpha (TNF-α), interleukin-6 (IL-6), and IL-1 revealed elevated levels of inflammation in the *Ts*-RNF group (Figure S8). Finally, we further examined how *Ts*-RNF affects autophagy-related signaling pathways. The level of phosphorylation Akt was lower in the *Ts*-RNF group than in the NC group as differentiation progressed. The expression of MAPK was upregulated during the early stage of differentiation, but downregulated during the late stage of differentiation. We

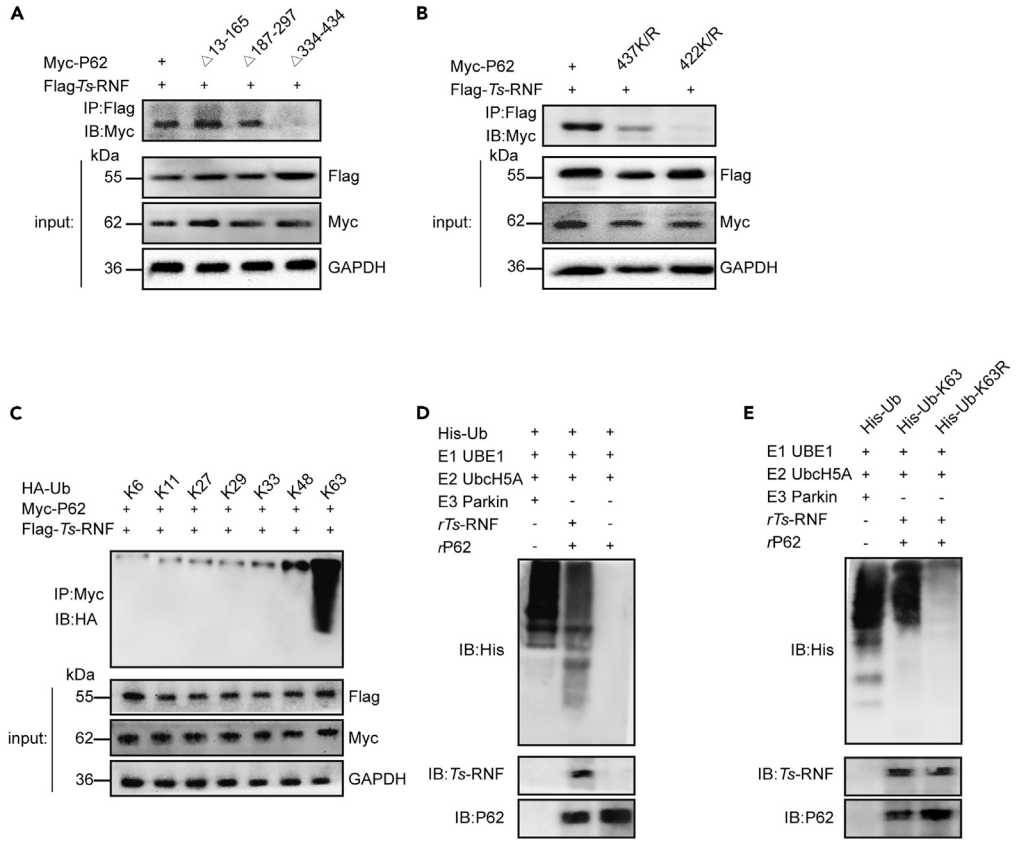

Figure 4. *Ts*-RNF interacts with SQSTM1/p62 K422 via K63 linker modification

(A) The Flag-*Ts*-RNF and Myc-p62, △13-165, △187-297, and △334-434 expression plasmids were cotransfected into HEK293T cells, and co-IP experiments were performed to determine the interaction between *Ts*-RNF and p62 using anti-FLAG beads followed by immunoblotting.

(B) The Flag-*Ts*-RNF and Myc-p62, 422K/R, and 437K/R expression plasmids were cotransfected into HEK293T cells, and co-IP experiments were performed with anti-FLAG beads followed by immunoblotting.

(C) The Flag-*Ts*-RNF, Myc-p62, and HA-Ub, K6, K11, K27, K29, K33, K48, and K63 expression plasmids were cotransfected into HEK293T cells, and co-IP experiments were performed to determine the ubiquitination linkage antibodies between *Ts*-RNF and p62 by anti-Myc beads followed by immunoblotting.

(D) The *in vitro* ubiquitination assay showing the interaction between *Ts*-RNF and p62. The *Ts*-RNF protein was incubated with HA-Ub, E1 (UBE1), E2 (UbcH5A), E3 (Parkin), and ATP buffer in the presence or absence of p62 protein at 37°C for 2 h. Parkin auto-ubiquitination reaction was utilized as a positive control. After the termination, the reaction mixture was subjected to SDS-PAGE and immunoblotting assay with an anti-HA antibody.

(E) *In vitro* ubiquitination assay showing K63-linked ubiquitin chains between *Ts*-RNF and p62. *Ts*-RNF and p62 protein were incubated with His-Ub (WT, K48, K63R), E1 (UBE1), E2 (UbcH5A), E3 (Parkin), and ATP buffer at 37°C for 2 h. Parkin auto-ubiquitination reaction was utilized as a positive control. After the termination, the reaction mixture was subjected to SDS-PAGE and immunoblotting assay with an anti-His antibody.

also observed abnormal levels of key proteins in the autophagy pathway, including mTOR and ULK1, in the *Ts*-RNF group (Figure 5F). These findings suggest that the direct interaction between *Ts*-RNF and p62 leads to the accumulation of p62, thereby inhibiting p62-mediated autophagy and impacting mitochondrial clearance and dynamics during differentiation.

RNAi targeting of the *Ts*-RNF gene affects the development of *T. spiralis*

To fully understand the impact of the interaction between *Ts*-RNF and p62 on helminth growth *in vivo* and explore its potential as a drug target for trichinosis, we used RNA interference (RNAi) to silence the *Ts*-RNF gene in *T. spiralis* and then injected NBL via the tail vein after interference. Electroporation was employed for the transfection of fluorescently labeled siRNA controls, which enabled the efficient delivery of siRNA into *T. spiralis*. Transfection of siRNA766 resulted in a significant reduction of both *Ts*-RNF gene and protein expression compared with that resulting from control siRNA transfection (Figures 6A and S9A). Subsequently, siRNA-*Ts*-NBL, *Ts*-NBL, and PBS were administered intravenously into mice via the tail vein. Mouse skeletal muscle samples were collected at three time points on days 3, 10, and 17 post-infection (Figure 6B). Subsequently, confocal immunofluorescence analysis was employed to assess the colocalization of *Ts*-RNF-p62 in mouse skeletal muscle on day 17 post-infection. Quantitative colocalization analysis was performed using ImageJ software to quantify the degree of fluorescence signal overlap. Colocalization between *Ts*-RNF and p62 was evident, whereas *T. spiralis* transfected with siRNA766 exhibited

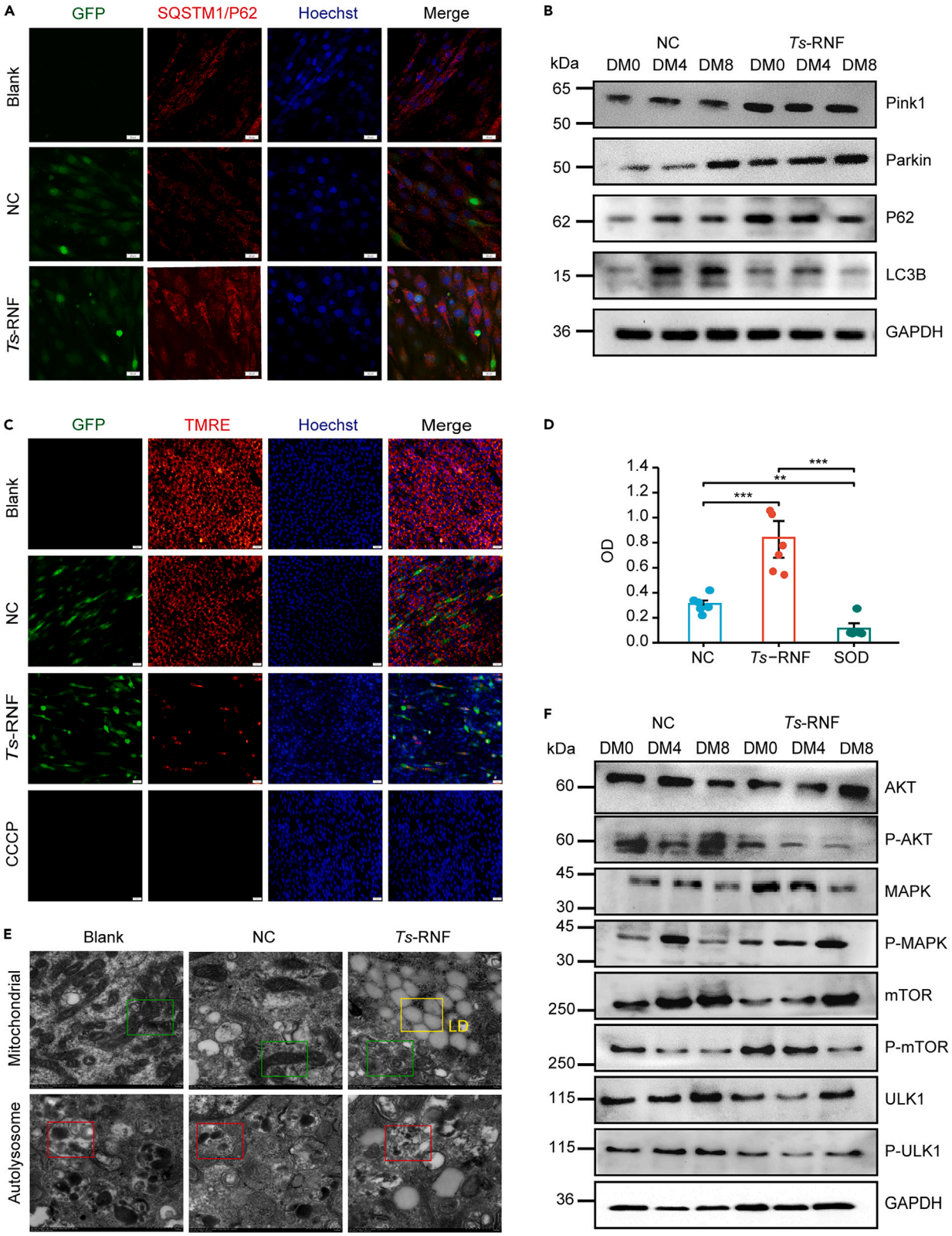
A
GFP
SQSTM1/P62
Hoechst
Merge
Blank
NC
Ts-RNF
B
NC
Ts-RNF
kDa
DM0 DM4 DM8 DM0 DM4 DM8
65
50
Pink1
50
Parkin
62
P62
15
LC3B
36
GAPDH
C
GFP
TMRE
Hoechst
Merge
Blank
NC
Ts-RNF
CCCP
D
OD
1.4
1.2
1.0
0.8
0.6
0.4
0.2
0.0
***
**
***
NC
Ts-RNF
SOD
E
Blank
NC
Ts-RNF
Mitochondrial
Autolysosome
LD
F
NC
Ts-RNF
kDa
DM0 DM4 DM8 DM0 DM4 DM8
60
AKT
60
P-AKT
45
30
MAPK
45
30
P-MAPK
250
mTOR
250
P-mTOR
115
ULK1
115
P-ULK1
36
GAPDH

Figure 5. *Ts*-RNF interacted with SQSTM1/p62 to influence mitochondrial clearance in C2C12 cells

(A) Confocal microscopy images of p62 on day 8 of differentiation. p62 (red), *Ts*-RNF (green), and Hoechst (blue). Untransfected cells (Blank) and cells transfected with empty vector served as negative controls (NC). Representative single optical sections and merged images are shown. Scale bars: 20 μm.

(B) Representative immunoblots of Pink1(PTEN induced putative kinase 1), Parkin (PARK2), P62(SQSTM1), and LC3B(MAP1LC3) at different time points in the NC and *Ts*-RNF groups.

(C) Confocal microscopy images of mitochondrial membrane potential on the day 8 of differentiation. *Ts*-RNF (green), TMRE, tetramethylrhodamine ethyl ester (red), and Hoechst (blue). Untransfected cells (Blank) and cells transfected with empty vector served as controls (NC). Carbonyl cyanide p-trifluoromethoxy-phenylhydrazone (CCCP, 25 μM), an uncoupler of mitochondrial oxidative phosphorylation, was used as a control for mitochondrial depolarization. Representative single optical sections and merged images are shown. Scale bars: 50 μm.

(D) Superoxide anion kit assay analyzed the superoxide anion production of *Ts*-RNF and NC group on day 8 of differentiation (OD: 450 nm). Superoxide dismutase (SOD) was used as a positive control. Data are shown as the means ± SEMs from three independent experiments (n = 3). Statistical analysis was performed using one-way ANOVA test. *$p < 0.05$, **$p < 0.01$, ***$p < 0.001$; ns, not significant.

(E) Transmission electron microscope (TEM) was used to analyze the structure of mitochondria and lysosomes on the day 8 of differentiation. Red frame: autolysosome (autolysosomes were identified as single-membrane structures containing cytoplasmic components at various stages of degradation), Green frame: mitochondrial (mitochondria were identified by their characteristics and cristae), Yellow frame: lipid droplets. Magnification: 5.0 k. Scale bar: 1 μm.

(F) Western blotting was used to detect the total protein expression and phosphorylation levels of AKT (protein kinase B), MAPK (mitogen-activated protein kinase), mTOR (mammalian target of rapamycin), ULK1 (Unc-51-like autophagy activating kinase 1) at different time points in the NC and *Ts*-RNF groups. The data and images are representative of at least three independent experiments. The samples were derived from the same experiment, and the blots were processed in parallel.

pronounced p62 accumulation and the loss of cyst integrity (Figure 6C). Western blotting analysis revealed a significant decrease in the protein level of *Ts*-RNF in the siRNA-*Ts* group compared with the *Ts*-ML group. The results also demonstrated a significant upregulation of the expression of LC3-II and p62 expression in the siRNA-*Ts* group, indicating promotion of the cellular autophagy process. The levels of the proteins Pink1 and Parkin were lower in the siRNA-*Ts* group than in the *Ts* group, indicating that myotube differentiation may have been altered during cyst formation after infection in the siRNA-*Ts* group (Figures 6D and S7B). The histopathology results indicate that NBL in the *Ts* group typically progressed to ML and forms cysts. In contrast, growth and development were impaired in the siRNA-*Ts* group, with an absence of discernible collagen wrapping cysts (Figure 6E). The ML burden in mice inoculated with siRNA-*Ts*-transfected ML was significantly reduced compared with the *Ts*-ML group (Figure S9B). The mRNA expression of the proinflammatory cytokines TNF-α, IL-1β, and IL-6 was upregulated in skeletal muscle tissue during the late stages of infection, potentially disrupting homeostasis at the parasite site due to impaired parasite development (Figure 6F). Finally, we further explored the impact of *Ts*-RNF gene knockdown on the autophagy pathway in skeletal muscle. The levels of AKT and MAPK were elevated in the siRNA-*Ts* group compared with those in the *Ts* group. However, there was no alteration observed in the overall expression of the mTOR proteins, whereas the levels of both total ULK1 and phosphorylated ULK1 exhibited an increase (Figures S9C and S9D). These findings indicate that *Ts*-RNF plays a crucial role in regulating host cell autophagy and maintaining local microenvironmental homeostasis.

DISCUSSION

The first-stage larvae of *T. spiralis* reside in a highly organized intracellular location. In this study, we elucidated the mechanism by which *Ts*-RNF interferes with the host ubiquitination pathway and inhibits selective autophagy, thereby affecting myoblast differentiation and promoting cyst formation. This is the first report on the function of *T. spiralis* E3 ligases and the first report of high ubiquitin expression levels in *T. spiralis*-infected muscle tissue. Cellular ubiquitin homeostasis is highly dynamic and tightly regulated. High expression of ubiquitin leads to developmental defects in tissues.[4,27] This finding suggested that the ubiquitin system plays a major role in the interaction between *T. spiralis* and the host by affecting the protein homeostasis in the local microenvironment and participating in cyst formation. RNAi targeting of the ubiquitin-modification pathway, which mediates an essential survival mechanism for eukaryotic proteins, results in extensive tissue degeneration and death.[28] Interference with the *Ts*-RNF gene resulted in an increase in cystic tissue accompanied by the infiltration of inflammatory cells. The aberrant autophagy marker p62 has been shown to increase the aggregation of ubiquitinated proteins degraded by autophagy and is always accompanied by the accumulation of p62, as well as the interaction of p62 with LC3.[29] The observed increase in p62 and Pink1/Parkin levels indicates that mitophagy/autophagy-mediated destabilization of p62 and Pink1/Parkin is impaired, and possibly the clearance of these proteins is blocked during the mitophagy process. The interaction also causes changes in ubiquitination levels surrounding the mitochondria. These results may be due to damage to the *T. spiralis* body, which affects the exchange of substances between *T. spiralis* and the host, resulting in the loss of excretion, the regulation of secreted products, and the reactivation of the immune response. These findings suggest that *Ts*-RNF plays an important regulatory role in endogenous ubiquitination in *T. spiralis* and is also critical for maintaining protein homeostasis in the host and helminth.

The p62 receptor protein functions as a pivotal regulator of intracellular signaling and interacts with diverse signal transducers to exert a profound influence on crucial physiological and pathological states.[30,31] Degenerative diseases are characterized by dominantly inherited missense or deletion mutations in the UBA domain of p62. The pathogenic mechanisms underlying these diseases involve disruptions in the binding between p62 and ubiquitin due to mutations in the UBA domain, resulting in the accumulation of p62 aggregates and ubiquitination inclusions.[32–34] According to our findings, the accumulation of p62 indicates a resemblance between the level of autophagy in muscle during the larval stage of *T. spiralis* infection and that during myopathy. The predominant lysine residues within the PB1 and UBA domains are responsible for multiple p62 ubiquitination sites.[35] TRAF6,[35] TRIM21,[36] RNF26[37] and other ubiquitin ligases can promote or hinder the

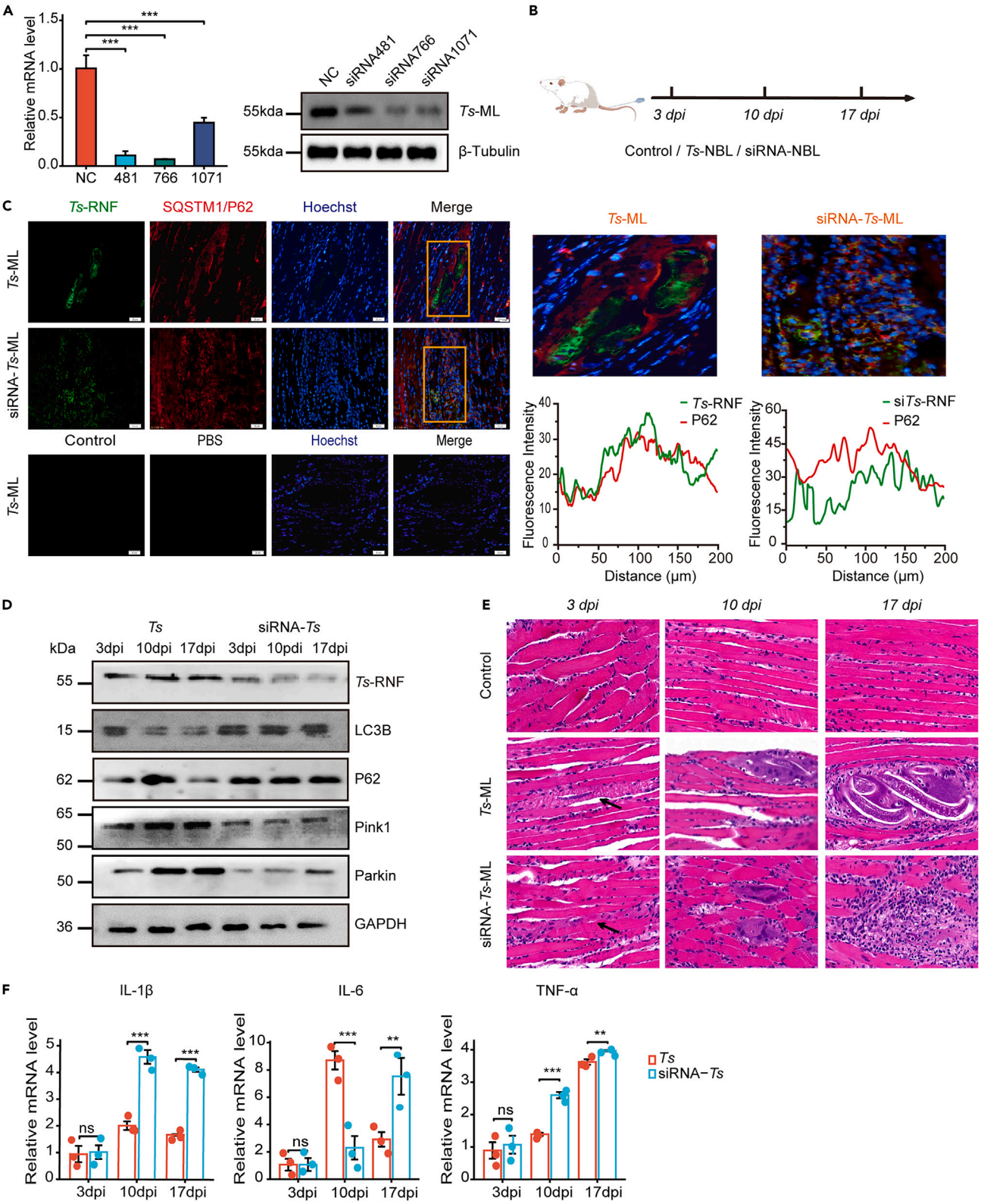
A
Relative mRNA level
1.5
1.0
0.5
0.0
NC
481
766
1071
***
***
***
NC
siRNA481
siRNA766
siRNA1071
55kda
Ts-ML
55kda
β-Tubulin
B
3 dpi
10 dpi
17 dpi
Control / Ts-NBL / siRNA-NBL
C
Ts-RNF
SQSTM1/P62
Hoechst
Merge
Ts-ML
siRNA-Ts-ML
Control
PBS
Hoechst
Merge
Ts-ML
Ts-ML
siRNA-Ts-ML
Ts-RNF
P62
Fluorescence Intensity
Distance (μm)
siTs-RNF
P62
Fluorescence Intensity
Distance (μm)
D
Ts
siRNA-Ts
kDa
3dpi
10dpi
17dpi
3dpi
10pdi
17dpi
55
Ts-RNF
15
LC3B
62
P62
65
50
Pink1
50
Parkin
36
GAPDH
E
3 dpi
10 dpi
17 dpi
Control
Ts-ML
siRNA-Ts-ML
F
IL-1β
IL-6
TNF-α
Relative mRNA level
ns
***
***
ns
***
**
ns
***
**
3dpi
10dpi
17dpi
Ts
siRNA−Ts

Figure 6. RNAi of the *Ts*-RNF gene affects the development and skeletal muscle autophagy level

(A) The protein expression levels of *Ts*-RNF after siRNA interference in each group were detected by *Ts*-RNF Rb pAb. Fluorescently labeled siRNA interference *Ts*-ML was used as a negative control (NC). The mRNA expression levels of the *Ts*-RNF gene after siRNA interference in each group after siRNA interference. Data are shown as the means ± SEMs from three independent experiments (n = 3). Statistical analysis was performed using one-way ANOVA test. *p < 0.05, **p < 0.01, ***p < 0.001; ns, not significant.

(B) Time points for tail vein injection to induce infection in different groups and mouse diaphragm collection.

(C) Confocal microscopy images of p62 in the skeletal muscle of the infected mice. p62 (red), *Ts*-RNF (green), and Hoechst (blue). Primary antibodies were replaced with preimmune serum, and PBS served as a control. Representative single optical sections and merged images are shown. Scale bars: 20 μm.

(D) The skeletal muscle of the mouse was collected on days 3, 10, and 17 after infection with *T. spiralis*. Western blotting was used to detect the total protein expression and phosphorylation levels of *Ts*-RNF, Pink1(PTEN induced putative kinase 1), Parkin (PARK2), P62(SQSTM1), and LC3B(MAP1LC3) in the *Ts* group and the siRNA-*Ts* group. The data and images are representative of at least three independent experiments. The samples were derived from the same experiment, and the blots were processed in parallel.

(E) H&E-stained sections of the mouse diaphragm on days 3, 10, and 17 after infection with *T. spiralis* with normal uninfected mouse skeletal muscle as a control. Scale bar: 20 μm.

(F) The skeletal muscle of mouse was collected on days 3, 10, and 17 after infection with *T. spiralis* and the mRNA expression levels of IL-1β, TNF-α, and IL-6 in the NC group and *Ts*-RNF group. Data are shown as the means ± SEMs from three independent experiments (n = 3). Statistical analysis was performed using independent samples t test. *p < 0.05, **p < 0.01, ***p < 0.001; ns, not significant.

oligomerization and activation of p62 through the use of different ubiquitination sites, thereby affecting its function. The conventional role of ubiquitination lies in the targeted degradation of substrate proteins by the 26S proteasome. However, the addition of K63-linked linear ubiquitin chains promotes signaling complex assembly via a nondegradable mechanism and may serve as a platform that facilitates protein-protein interactions in signal transduction.[38] The p62 bodies exhibit an enrichment of polyubiquitin chains and display preferential recruitment of K63-linked polyubiquitin chains.[39] Furthermore, loss of the PB1 domain impairs p62 self-binding, whereas loss of the UBA domain hinders p62 body formation even if the PB1 domain remains intact.[39] The initiation of ubiquitin-mediated selective autophagy is believed to occur through the recognition of ubiquitinated proteins by the C-terminal UBA domain of p62. The p62 UBA domain exists in a dynamic equilibrium between dimeric and monomeric states and undergoes autoinhibition for efficient binding to ubiquitin.[32] In our study, *Ts*-RNF was shown to interact with the UBA domain of p62. This ubiquitin may enhance ubiquitin binding by interfering with dimerization, thereby affecting the dimer-monomer balance and the Ub-binding function of p62 indirectly, although this hypothesis requires further confirmation. We will next study whether ubiquitination at K422 affects the formation of ubiquitinated inclusion bodies and reduces LC3 interaction and cell viability and what roles these functions play in tissues colonized by pathogens.

The conversion of host striated muscle cells into cysts is a critical adaptive process following *T. spiralis* infection that occurs over up to 20 days from initial larval invasion to cyst formation.[4,40] Mitochondrial clearance, remodeling, and myotube differentiation occur sequentially during skeletal muscle differentiation.[41,42] The accumulation of dysfunctional mitochondria results in tissue damage.[43,44] During differentiation, specific induction of p62 in the cytoplasm is essential for mitochondrial clearance, and p62 accumulation in the absence of autophagy impairs myoblast differentiation.[45] We identified a potential mechanism through which *Ts*-RNF interacts with p62 and impairs the ability of host cells to efficiently eliminate damaged mitochondria. This disruption of cellular homeostasis contributes to the establishment of a pathogenic parasite environment. In recent years, an increasing number of studies have shown that certain pathogens can directly or indirectly induce mitophagy and regulate this process through diverse mechanisms, thereby disrupting cellular homeostasis and facilitating persistent infection.[46–48] Host cell autophagy induced by *Toxoplasma gondii* and *Plasmodium* is induced by parasites, which collect nutrients and aid in their growth and development.[49,50] *T. spiralis* regulates the induction and inhibition of autophagy, but the exact mechanism and results of these changes in the process of autophagy have not been fully elucidated. After mitochondrial substrate proteins are ubiquitinated, inhibitory mechanisms interfere with the formation and extension of their ubiquitin chains or the binding of ubiquitinated proteins to cargo proteins, thereby affecting the subsequent regulation of autophagy.[51–53] When mitochondrial clearance is blocked, we can infer that this process may provide energy to promote reproductive development. Interestingly, in our study, we identified many lipid droplets in the cytoplasm. Selective phagocytosis of lipid droplets is also mediated by autophagy, and p62 is a potential receptor for lipid droplet turnover.[54] Notably, such changes in mitophagy and lipid metabolism may be related to the formation of collagen tissue around the cyst.

T. spiralis effector interactions with the host are multifaceted, dynamic processes that are coordinated by the pathogen and host in both time and space.[55] Understanding the molecular basis of ubiquitination in the parasite and host immune systems may yield effective approaches to augment host defenses and prevent disruptions immunological homeostasis. We have elucidated a mechanism by which *Ts*-RNF disrupts the host ubiquitination pathway and may affect host autophagy, thereby impairing myoblast differentiation and promoting cyst formation as a countermeasure against host defense mechanism.

Limitations of this study

These findings of this study have considerable implications for understanding the developmental process of *T. spiralis* cyst formation. *T. spiralis* has a complex life cycle, and the parasite cannot infect host cells under laboratory conditions; therefore, fully replicating the functions of natural proteins during a natural infection is challenging. Nevertheless, we established a stably transfected cell line and conducted detailed studies of protein functions and substrates. Myoblast differentiation is a mature model method that is capable of simulating repair responses after injury *in vitro*, but further research is needed to investigate the multicellular interactions between *T. spiralis* naturally during

persistent infection. Additionally, limitations associated with *T. spiralis* gene knockout technology also restrict our understanding of E3 ligase function.

STAR★METHODS

Detailed methods are provided in the online version of this paper and include the following:

- KEY RESOURCES TABLE
- RESOURCE AVAILABILITY
  - Lead contact
  - Materials availability
  - Data and code availability
- EXPERIMENTAL MODEL AND STUDY PARTICIPANT DETAILS
  - ML-ES sample preparation
  - Cell culture and induction of differentiation
  - *T. spiralis* RNAi
- METHOD DETAILS
  - Transfection
  - Immunofluorescence analysis
  - Quantitative proteomic analysis of ubiquitination
  - Co-IP assays for analysis of protein–protein interactions
  - Ubiquitination assays
  - Quantitative real-time PCR
  - Western blot analysis
  - Mitochondrial membrane potential and superoxide anion assays
  - TEM
  - Ethics
- QUANTIFICATION AND STATISTICAL ANALYSIS

SUPPLEMENTAL INFORMATION

Supplemental information can be found online at https://doi.org/10.1016/j.isci.2024.109102.

ACKNOWLEDGMENTS

We thank PTM Biolabs (Hangzhou, China) for their assistance in the quantitative proteomic LC-MS/MS analysis of ubiquitination modification.

This study was supported by The National Key Research and Development Program of China (2021YFC2600202) and the National Natural Science Foundation of China (NSFC32230104, NSFC32202835, NSFC82201959).

AUTHOR CONTRIBUTIONS

Conceptualization, X.L., M.L., P.B., and I.V.; methodology, J.D.P. and X.J.; investigation, J.D.P., Z.D., and Y.L.; writing—original draft, J.D.P. and Y.L.; writing—review and editing, N.X. and J.D.; supervision, X.L. and N.X.; funding acquisition, X.L. and M.L.

DECLARATION OF INTERESTS

The authors declare no competing interest.

Received: October 6, 2023
Revised: November 5, 2023
Accepted: January 30, 2024
Published: February 2, 2024

REFERENCES

1. Bai, X., Hu, X., Liu, X., Tang, B., and Liu, M. (2017). Current Research of Trichinellosis in China. Front. Microbiol. *8*, 1472. https://doi.org/10.3389/fmicb.2017.01472.
2. Hernández-Ancheyta, L., Salinas-Tobón, M.D.R., Cifuentes-Goches, J.C., and Hernández-Sánchez, J. (2018). Trichinella spiralis muscle larvae excretory-secretory products induce changes in cytoskeletal and myogenic transcription factors in primary myoblast cultures. Int. J. Parasitol. *48*, 275–285. https://doi.org/10.1016/j.ijpara.2017.10.002.
3. Dvorožňáková, E., Hurníková, Z., and Kołodziej-Sobocińska, M. (2011). Development of cellular immune response of mice to infection with low doses of Trichinella spiralis, Trichinella britovi and Trichinella pseudospiralis larvae. Parasitol. Res. *108*, 169–176. https://doi.org/10.1007/s00436-010-2049-x.
4. Wu, Z., Sofronic-Milosavljevic, L., Nagano, I., and Takahashi, Y. (2008). Trichinella spiralis: nurse cell formation with emphasis on

analogy to muscle cell repair. Parasit. Vectors *1*, 27. https://doi.org/10.1186/1756-3305-1-27.

5. Bai, X., Wu, X., Wang, X., Liu, X., Song, Y., Gao, F., Miao, Y., Yu, L., Tang, B., Wang, X., et al. (2012). Inhibition of mammalian muscle differentiation by excretory secretory products of muscle larvae of Trichinella spiralis in vitro. Parasitol. Res. *110*, 2481–2490. https://doi.org/10.1007/s00436-011-2789-2.
6. Bai, X., Wang, X.L., Tang, B., Shi, H.N., Boireau, P., Rosenthal, B., Wu, X.P., Liu, M.Y., and Liu, X.L. (2016). The roles of supernatant of macrophage treated by excretory-secretory products from muscle larvae of Trichinella spiralis on the differentiation of C2C12 myoblasts. Vet. Parasitol. *231*, 83–91. https://doi.org/10.1016/j.vetpar.2016.07.033.
7. Hu, X., Liu, X., Bai, X., Yang, L., Ding, J., Jin, X., Li, C., Zhang, Y., Li, Y., Yang, Y., and Liu, M. (2021). Effects of Trichinella spiralis and its excretory/secretory products on autophagy of host muscle cells in vivo and in vitro. PLoS Negl. Trop. Dis. *15*, e0009040. https://doi.org/10.1371/journal.pntd.0009040.
8. Song, L., and Luo, Z.Q. (2019). Post-translational regulation of ubiquitin signaling. J. Cell Biol. *218*, 1776–1786. https://doi.org/10.1083/jcb.201902074.
9. Ashida, H., and Sasakawa, C. (2017). Bacterial E3 ligase effectors exploit host ubiquitin systems. Curr. Opin. Microbiol. *35*, 16–22. https://doi.org/10.1016/j.mib.2016.11.001.
10. Furukawa, M., Andrews, P.S., and Xiong, Y. (2005). Assays for RING family ubiquitin ligases. Methods Mol. Biol. *301*, 37–46. https://doi.org/10.1385/1-59259-895-1:037.
11. Jiang, X., and Chen, Z.J. (2011). The role of ubiquitylation in immune defence and pathogen evasion. Nat. Rev. Immunol. *12*, 35–48. https://doi.org/10.1038/nri3111.
12. Zheng, Z., Wei, C., Guan, K., Yuan, Y., Zhang, Y., Ma, S., Cao, Y., Wang, F., Zhong, H., and He, X. (2016). Bacterial E3 Ubiquitin Ligase IpaH4.5 of Shigella flexneri Targets TBK1 To Dampen the Host Antibacterial Response. J. Immunol. *196*, 1199–1208. https://doi.org/10.4049/jimmunol.1501045.
13. Bullones-Bolaños, A., Araujo-Garrido, J.L., Fernández-García, J., Romero, F., Bernal-Bayard, J., and Ramos-Morales, F. (2022). SNRPD2 Is a Novel Substrate for the Ubiquitin Ligase Activity of the Salmonella Type III Secretion Effector SlrP. Biology *11*, 1517. https://doi.org/10.3390/biology11101517.
14. Qiu, J., Sheedlo, M.J., Yu, K., Tan, Y., Nakayasu, E.S., Das, C., Liu, X., and Luo, Z.Q. (2016). Ubiquitination independent of E1 and E2 enzymes by bacterial effectors. Nature *533*, 120–124. https://doi.org/10.1038/nature17657.
15. Lin, Y.H., and Machner, M.P. (2017). Exploitation of the host cell ubiquitin machinery by microbial effector proteins. J. Cell Sci. *130*, 1985–1996. https://doi.org/10.1242/jcs.188482.
16. Li, J., Chai, Q.Y., and Liu, C.H. (2016). The ubiquitin system: a critical regulator of innate immunity and pathogen-host interactions. Cell. Mol. Immunol. *13*, 560–576. https://doi.org/10.1038/cmi.2016.40.
17. Maizels, R.M., Smits, H.H., and McSorley, H.J. (2018). Modulation of Host Immunity by Helminths: The Expanding Repertoire of Parasite Effector Molecules. Immunity *49*, 801–818. https://doi.org/10.1016/j.immuni.2018.10.016.
18. Hashimoto, M., Murata, E., and Aoki, T. (2010). Secretory protein with RING finger domain (SPRING) specific to Trypanosoma cruzi is directed, as a ubiquitin ligase related protein, to the nucleus of host cells. Cell Microbiol. *12*, 19–30. https://doi.org/10.1111/j.1462-5822.2009.01375.x.
19. Nair, S.C., Xu, R., Pattaradilokrat, S., Wu, J., Qi, Y., Zilversmit, M., Ganesan, S., Nagarajan, V., Eastman, R.T., Orandle, M.S., et al. (2017). A Plasmodium yoelii HECT-like E3 ubiquitin ligase regulates parasite growth and virulence. Nat. Commun. *8*, 223. https://doi.org/10.1038/s41467-017-00267-3.
20. White, R.R., Ponsford, A.H., Weekes, M.P., Rodrigues, R.B., Ascher, D.B., Mol, M., Selkirk, M.E., Gygi, S.P., Sanderson, C.M., and Artavanis-Tsakonas, K. (2016). Ubiquitin-Dependent Modification of Skeletal Muscle by the Parasitic Nematode, Trichinella spiralis. PLoS Pathog. *12*, e1005977. https://doi.org/10.1371/journal.ppat.1005977.
21. Liu, X., Feng, Y., Bai, X., Wang, X., Qin, R., Tang, B., Yu, X., Yang, Y., Liu, M., and Gao, F. (2021). Comparative multi-omics analyses reveal differential expression of key genes relevant for parasitism between non-encapsulated and encapsulated Trichinella. Commun. Biol. *4*, 134. https://doi.org/10.1038/s42003-021-01650-z.
22. Song, G., Liu, B., Li, Z., Wu, H., Wang, P., Zhao, K., Jiang, G., Zhang, L., and Gao, C. (2016). E3 ubiquitin ligase RNF128 promotes innate antiviral immunity through K63-linked ubiquitination of TBK1. Nat. Immunol. *17*, 1342–1351. https://doi.org/10.1038/ni.3588.
23. Montarras, D., L'honoré, A., and Buckingham, M. (2013). Lying low but ready for action: the quiescent muscle satellite cell. FEBS J. *280*, 4036–4050. https://doi.org/10.1111/febs.12372.
24. Sciorati, C., Rigamonti, E., Manfredi, A.A., and Rovere-Querini, P. (2016). Cell death, clearance and immunity in the skeletal muscle. Cell Death Differ. *23*, 927–937. https://doi.org/10.1038/cdd.2015.171.
25. Heidelberger, J.B., Voigt, A., Borisova, M.E., Petrosino, G., Ruf, S., Wagner, S.A., and Beli, P. (2018). Proteomic profiling of VCP substrates links VCP to K6-linked ubiquitylation and c-Myc function. EMBO Rep. *19*, e44754. https://doi.org/10.15252/embr.201744754.
26. Rayner, S.L., Morsch, M., Molloy, M.P., Shi, B., Chung, R., and Lee, A. (2019). Using proteomics to identify ubiquitin ligase-substrate pairs: how novel methods may unveil therapeutic targets for neurodegenerative diseases. Cell. Mol. Life Sci. *76*, 2499–2510. https://doi.org/10.1007/s00018-019-03082-9.
27. Hoe, N., Huang, C.M., Landis, G., Verhage, M., Ford, D., Yang, J., van Leeuwen, F.W., and Tower, J. (2011). Ubiquitin over-expression phenotypes and ubiquitin gene molecular misreading during aging in Drosophila melanogaster. Aging (Albany NY) *3*, 237–261. https://doi.org/10.18632/aging.100278.
28. Wang, J., Paz, C., Padalino, G., Coghlan, A., Lu, Z., Gradinaru, I., Collins, J.N.R., Berriman, M., Hoffmann, K.F., and Collins, J.J., 3rd (2020). Large-scale RNAi screening uncovers therapeutic targets in the parasite Schistosoma mansoni. Science *369*, 1649–1653. https://doi.org/10.1126/science.abb7699.
29. Shivalingappa, P.C., Hole, R., Westphal, C.V., and Vij, N. (2016). Airway Exposure to E-Cigarette Vapors Impairs Autophagy and Induces Aggresome Formation. Antioxid. Redox Signal. *24*, 186–204. https://doi.org/10.1089/ars.2015.6367.
30. Sánchez-Martín, P., and Komatsu, M. (2018). p62/SQSTM1-steering the cell through health and disease. J. Cell Sci. *131*, jcs222836. https://doi.org/10.1242/jcs.222836.
31. Katsuragi, Y., Ichimura, Y., and Komatsu, M. (2015). p62/SQSTM1 functions as a signaling hub and an autophagy adaptor. FEBS J. *282*, 4672–4678. https://doi.org/10.1111/febs.13540.
32. Isogai, S., Morimoto, D., Arita, K., Unzai, S., Tenno, T., Hasegawa, J., Sou, Y.S., Komatsu, M., Tanaka, K., Shirakawa, M., and Tochio, H. (2011). Crystal structure of the ubiquitin-associated (UBA) domain of p62 and its interaction with ubiquitin. J. Biol. Chem. *286*, 31864–31874. https://doi.org/10.1074/jbc.M111.259630.
33. Bucelli, R.C., Arhzaouy, K., Pestronk, A., Pittman, S.K., Rojas, L., Sue, C.M., Evilä, A., Hackman, P., Udd, B., Harms, M.B., and Weihl, C.C. (2015). SQSTM1 splice site mutation in distal myopathy with rimmed vacuoles. Neurology *85*, 665–674. https://doi.org/10.1212/WNL.0000000000001864.
34. Rea, S.L., Majcher, V., Searle, M.S., and Layfield, R. (2014). SQSTM1 mutations–bridging Paget disease of bone and ALS/FTLD. Exp. Cell Res. *325*, 27–37. https://doi.org/10.1016/j.yexcr.2014.01.020.
35. Pan, J.A., Sun, Y., Jiang, Y.P., Bott, A.J., Jaber, N., Dou, Z., Yang, B., Chen, J.S., Catanzaro, J.M., Du, C., et al. (2016). TRIM21 Ubiquitylates SQSTM1/p62 and Suppresses Protein Sequestration to Regulate Redox Homeostasis. Mol. Cell *62*, 149–151. https://doi.org/10.1016/j.molcel.2016.03.015.
36. Heath, R.J., Goel, G., Baxt, L.A., Rush, J.S., Mohanan, V., Paulus, G.L.C., Jani, V., Lassen, K.G., and Xavier, R.J. (2016). RNF166 Determines Recruitment of Adaptor Proteins during Antibacterial Autophagy. Cell Rep. *17*, 2183–2194. https://doi.org/10.1016/j.celrep.2016.11.005.
37. Cremer, T., Jongsma, M.L.M., Trulsson, F., Vertegaal, A.C.O., Neefjes, J., and Berlin, I. (2021). The ER-embedded UBE2J1/RNF26 ubiquitylation complex exerts spatiotemporal control over the endolysosomal pathway. Cell Rep. *34*, 108659. https://doi.org/10.1016/j.celrep.2020.108659.
38. Hu, H., and Sun, S.C. (2016). Ubiquitin signaling in immune responses. Cell Res. *26*, 457–483. https://doi.org/10.1038/cr.2016.40.
39. Lee, Y., Chou, T.F., Pittman, S.K., Keith, A.L., Razani, B., and Weihl, C.C. (2017). Keap1/Cullin3 Modulates p62/SQSTM1 Activity via UBA Domain Ubiquitination. Cell Rep. *20*, 1994. https://doi.org/10.1016/j.celrep.2017.08.019.
40. Dumont, N.A., Bentzinger, C.F., Sincennes, M.C., and Rudnicki, M.A. (2015). Satellite Cells and Skeletal Muscle Regeneration. Compr. Physiol. *5*, 1027–1059. https://doi.org/10.1002/cphy.c140068.
41. Ju, J.S., Varadhachary, A.S., Miller, S.E., and Weihl, C.C. (2010). Quantitation of "autophagic flux" in mature skeletal muscle. Autophagy *6*, 929–935. https://doi.org/10.4161/auto.6.7.12785.
42. McMillan, E.M., and Quadrilatero, J. (2014). Autophagy is required and protects against apoptosis during myoblast differentiation. Biochem. J. *462*, 267–277. https://doi.org/10.1042/bj20140312.

43. Sin, J., Andres, A.M., Taylor, D.J.R., Weston, T., Hiraumi, Y., Stotland, A., Kim, B.J., Huang, C., Doran, K.S., and Gottlieb, R.A. (2016). Mitophagy is required for mitochondrial biogenesis and myogenic differentiation of C2C12 myoblasts. Autophagy *12*, 369–380. https://doi.org/10.1080/15548627.2015.1115172.
44. Parousis, A., Carter, H.N., Tran, C., Erlich, A.T., Mesbah Moosavi, Z.S., Pauly, M., and Hood, D.A. (2018). Contractile activity attenuates autophagy suppression and reverses mitochondrial defects in skeletal muscle cells. Autophagy *14*, 1886–1897. https://doi.org/10.1080/15548627.2018.1491488.
45. Sakuma, K., Kinoshita, M., Ito, Y., Aizawa, M., Aoi, W., and Yamaguchi, A. (2016). p62/SQSTM1 but not LC3 is accumulated in sarcopenic muscle of mice. J. Cachexia Sarcopenia Muscle *7*, 204–212. https://doi.org/10.1002/jcsm.12045.
46. Zhang, L., Qin, Y., and Chen, M. (2018). Viral strategies for triggering and manipulating mitophagy. Autophagy *14*, 1665–1673. https://doi.org/10.1080/15548627.2018.1466014.
47. Ding, B., Zhang, L., Li, Z., Zhong, Y., Tang, Q., Qin, Y., and Chen, M. (2017). The Matrix Protein of Human Parainfluenza Virus Type 3 Induces Mitophagy that Suppresses Interferon Responses. Cell Host Microbe *21*, 538–547.e4. https://doi.org/10.1016/j.chom.2017.03.004.
48. Zhang, Y., Yao, Y., Qiu, X., Wang, G., Hu, Z., Chen, S., Wu, Z., Yuan, N., Gao, H., Wang, J., et al. (2019). Listeria hijacks host mitophagy through a novel mitophagy receptor to evade killing. Nat. Immunol. *20*, 433–446. https://doi.org/10.1038/s41590-019-0324-2.
49. Rawat, R.S., Bansal, P., and Sharma, P. (2022). A VPS15-like kinase regulates apicoplast biogenesis and autophagy by promoting PI3P generation in Toxoplasma gondii. PLoS Pathog. *18*, e1010922. https://doi.org/10.1371/journal.ppat.1010922.
50. Schroeder, E.A., Chirgwin, M.E., and Derbyshire, E.R. (2022). Plasmodium's fight for survival: escaping elimination while acquiring nutrients. Trends Parasitol. *38*, 544–557. https://doi.org/10.1016/j.pt.2022.04.004.
51. Green, D.R., and Levine, B. (2014). To be or not to be? How selective autophagy and cell death govern cell fate. Cell *157*, 65–75. https://doi.org/10.1016/j.cell.2014.02.049.
52. Yao, R.Q., Ren, C., Xia, Z.F., and Yao, Y.M. (2021). Organelle-specific autophagy in inflammatory diseases: a potential therapeutic target underlying the quality control of multiple organelles. Autophagy *17*, 385–401. https://doi.org/10.1080/15548627.2020.1725377.
53. Baechler, B.L., Bloemberg, D., and Quadrilatero, J. (2019). Mitophagy regulates mitochondrial network signaling, oxidative stress, and apoptosis during myoblast differentiation. Autophagy *15*, 1606–1619. https://doi.org/10.1080/15548627.2019.1591672.
54. Lee, S.J., Pfluger, P.T., Kim, J.Y., Nogueiras, R., Duran, A., Pagès, G., Pouysségur, J., Tschöp, M.H., Diaz-Meco, M.T., and Moscat, J. (2010). A functional role for the p62-ERK1 axis in the control of energy homeostasis and adipogenesis. EMBO Rep. *11*, 226–232. https://doi.org/10.1038/embor.2010.7.
55. Schmid-Hempel, P. (2008). Parasite immune evasion: a momentous molecular war. Trends Ecol. Evol. *23*, 318–326. https://doi.org/10.1016/j.tree.2008.02.011.
56. Pang, J., Ding, J., Zhang, L., Zhang, Y., Yang, Y., Bai, X., Liu, X., Jin, X., Guo, H., Yang, Y., and Liu, M. (2020). Effect of recombinant serine protease from adult stage of Trichinella spiralis on TNBS-induced experimental colitis in mice. Int. Immunopharmacol. *86*, 106699. https://doi.org/10.1016/j.intimp.2020.106699.
57. Song, G., Liu, B., and Gao, C. (2019). E3 ubiquitin ligase RNF128 promotes innate antiviral immunity through K63-linked ubiquitination of TBK1. Eur. J. Immunol. *49*, 82.

STAR★METHODS

KEY RESOURCES TABLE

REAGENT or RESOURCE	SOURCE	IDENTIFIER
Antibodies		
Anti-MyoD1Rabbit Polyclonal Antibody	absin, China	Cat#abs124179
Rabbit anti-MYOG Polyclonal Antibody	absin, China	Cat#abs137750
Anti-Myosin Heavy Chain antibody	Abcam, UK	Cat#ab37484; RRID:AB_2921304
Anti-Tubulin Antibody	Affinity, China	Cat#T0023; RRID:AB_2813772
Anti-Ubiquitin Rabbit mAb	PTM Biolabs, China	Cat#1106RM
Anti-HA tag Rabbit mAb	PTM Biolabs, China	Cat#5389
Anti-Flag tag Rabbit mAb	PTM Biolabs, China	Cat#5577
Anti-Myc tag Rabbit mAb	PTM Biolabs, China	Cat#5390
anti-phospho-Nf-κb (Ser536) Rabbit mAb	Cell Signaling Technology, USA	Cat#4025; RRID:AB_10827881
anti-PINK1 Rabbit mAb	Cell Signaling Technology, USA	Cat#6946; RRID:AB_11179069
Anti-parkin (D4Z1W) Rabbit mAb	Cell Signaling Technology, USA	Cat#32833; RRID:AB_3073958
anti-GAPDH antibody	Abcam, UK	Cat#ab8245; RRID;AB_2107448
Anti-lc3b antibody	Abcam, UK	Cat#ab192890; RRID:AB_2827794
anti-SQSTM1/p62 antibody	Abcam, UK	Cat#ab109012; RRID:AB_2810880
p38 MAPK Antibody	Affinity Biosciences, China	Cat#AF6456; RRID:AB_2835277
Phospho-p38 MAPK (Thr180/Tyr182) Antibody	Affinity Biosciences, China	Cat#AF4001; RRID:AB_2835330
Akt (pan) (C67E7) Rabbit mAb	Cell Signaling Technology, USA	Cat#4691; RRID:AB_915783
Phospho-Akt (Ser473) (D9E) XP Rabbit mAb	Cell Signaling Technology, USA	Cat#4060; RRID:AB_2315049
Anti- ULK1 antibody	Cell Signaling Technology, USA	Cat#4773; RRID:AB_2288252
Phospho-ULK1 (Ser757) (D7O6U) Rabbit mAb	Cell Signaling Technology, USA	Cat#14202; RRID:AB_2665508
mTOR (7C10) Rabbit mAb	Cell Signaling Technology, USA	Cat#2983; RRID:AB_2105622
Phospho-mTOR (Ser2448) (D9C2) XP Rabbit mAb	Cell Signaling Technology, USA	Cat#5536; RRID:AB_10691552
goat anti-rabbit IgG Alexa Fluor 555	Abcam, UK	Cat#ab150134; RRID:AB_2715537
HRP-linked anti-rabbit IgG antibody	Cell Signaling Technology, USA	Cat#7074; RRID:AB_2099233
Biological samples		
T. spiralis	The Laboratory	ISS534
Chemicals, peptides, and recombinant proteins		
Ubiquitin Conjugation Reaction Buffer Kit	Boston Biochem, USA	Cat#SK-10
Ubiquitin E1 Enzyme UBE1	Boston Biochem, USA	Cat#E−304
Ubiquitin E2 Enzyme UbcH7	Boston Biochem, USA	Cat#E2-640
Ubiquitin E3 Enzyme Parkin	Boston Biochem, USA	Cat#E3-160
HA Ubiquitin	Boston Biochem, USA	Cat#U-110
DMEM	Gibco, USA	Cat#11971025
FBS	Gibco, USA	Cat#11971025
HS	Gibco, USA	Cat#16050122
Lipofectamine 2000 reagent	Thermo Fisher Scientific, USA	Cat#11668019
Opti-MEM	Gibco, USA	Cat#31985062
MG132	MCE, China	Cat#HY-13259
DYKDDDDK Affinity Resin	Thermo Fisher Scientific, USA	Cat#A36801
TNT Quick Coupled Transcription/Translation System	Promega, USA	Cat#L1711
RNAiso Plus	TaKaRa, JPN	Cat#9109
X-treme GENE HP DNA transfection reagent	Roche, Germany	Cat#6366244001

(*Continued on next page*)

Continued

REAGENT or RESOURCE	SOURCE	IDENTIFIER
Critical commercial assays		
ubiquitin-modified proteomics and MS	PTM Biolabs, China	
Experimental models: Cell lines		
Human: HEK293T	ATCC	Cat# CRL-3216
Mouse: C2C12 ATCC	ATCC	Cat# CRL-1772
Experimental models: Organisms/strains		
Mouse: BALB/c mice	Laboratory Animal Center, Bethune Medical College, Jilin University	N/A
Ts-RNF lentiviral vector	Sangon Biotech, China	
Oligonucleotides		
Flag-*Ts*-RNF	Sangon Biotech, China	N/A
Myc-P62	Sangon Biotech, China	N/A
Myc- △ 13-165	Sangon Biotech, China	N/A
Myc- △ 187-297	Sangon Biotech, China	N/A
Myc- △ 334-434	Sangon Biotech, China	N/A
Myc-K422R	Sangon Biotech, China	N/A
Myc-K437R	Sangon Biotech, China	N/A
HA-Ub	Sangon Biotech, China	N/A
HA-K6	Sangon Biotech, China	N/A
HA-K11	Sangon Biotech, China	N/A
HA-K27	Sangon Biotech, China	N/A
HA-K29	Sangon Biotech, China	N/A
HA-K33	Sangon Biotech, China	N/A
HA-K48	Sangon Biotech, China	N/A
HA-K63	Sangon Biotech, China	N/A
Recombinant DNA		
TGTTGCTGCTGATCCGTCTGAAC	Sangon Biotech, China	*Ts*-RNF-F
ATGGGAGTTGCGTTGTCGTTGG	Sangon Biotech, China	*Ts*-RNF-R
GTGCTGATTACGCTGTTG	Sangon Biotech, China	*Ts*-GAPDH F
CTAAGCCATTGGTAGTGC	Sangon Biotech, China	*Ts*-GAPDH R
ATCATTGACCGCTCCTTTAGGT	Sangon Biotech, China	ki67-F
GCTCGCCTTGATGGTTCCT	Sangon Biotech, China	ki67-R
CCACTCCGGGACATAGACTTG	Sangon Biotech, China	MyoD-F
AAAAGCGCAGGTCTGGTGAG	Sangon Biotech, China	MyoD-R
GCTCAGTCCGCTCATAGCC	Sangon Biotech, China	MyoG-F
GCTCAGTCCGCTCATAGCC	Sangon Biotech, China	MyoG-R
GCGAATCGAGGCTCAGAACAA	Sangon Biotech, China	MyHC-F
GTAGTTCCGCCTTCGGTCTTG	Sangon Biotech, China	MyHC-R
GTTAGAACTGGTGAGCAGGAG	Sangon Biotech, China	Myomixer-F
CCATCGGGAGCAATGGAA	Sangon Biotech, China	Myomixer-R
CCTGCTGTCTCTCCCAAG	Sangon Biotech, China	Myomarker-F
AGAACCAGTGGGTCCCTAA	Sangon Biotech, China	Myomarker-R
GCCATGTACGTAGCCATCCA	Sangon Biotech, China	β-actin-F
ACGCTCGGTCAGGATCTTCA	Sangon Biotech, China	β-actin-R

(*Continued on next page*)

Continued

REAGENT or RESOURCE	SOURCE	IDENTIFIER
CTTCTTGGGACTGATGCTGGTGAC	Sangon Biotech, China	IL-6 -F
TCTGTTGGGAGTGGTATCCTCTGTG	Sangon Biotech, China	IL-6 -R
CGCTCTTCTGTCTACTGAACTTCGG	Sangon Biotech, China	TNF-α F
GTGGTTTGTGAGTGTGAGGGTCTG	Sangon Biotech, China	TNF-α R
CACTACAGGCTCCGAGATGAACAAC	Sangon Biotech, China	IL-1β F
TGTCGTTGCTTGGTTCTCCTTGTAC	Sangon Biotech, China	IL-1β R
AGGAAUUGUAACUUUCUUCUC	Sangon Biotech, China	siRNA-481 F
GAAGAAAGUUACAAUUCCUGC	Sangon Biotech, China	siRNA-481 R
GCAAUUUGCCUAGAAGAUUTT	Sangon Biotech, China	siRNA-766 F
AAUCUUCUAGGCAAAUUGCTT	Sangon Biotech, China	siRNA-766 R
AAAAUGUUGAAUUUCCUACCU	Sangon Biotech, China	siRNA-1071 R
GUAGGAAAUUCAACAUUUUAC	Sangon Biotech, China	siRNA-1071 R
Software and algorithms		
Prism	https://graphpad.com:443/scientific-software/prism/	GraphPad

RESOURCE AVAILABILITY

Lead contact

Further information and requests for resources and reagents should be directed to and will be fulfilled by the Lead Contact, Xiao lei Liu (liuxlei@163.com).

Materials availability

This study did not generate new unique reagents.

Data and code availability

- All data reported in this paper will be shared by the lead contact upon request.
- This paper does not report original code.
- Any additional information required to reanalyze the data reported in this paper is available from the lead contact upon request.

EXPERIMENTAL MODEL AND STUDY PARTICIPANT DETAILS

ML-ES sample preparation

ML-ES were collected at 30 dpi from experimentally infected *T. spiralis* (ISS534) collected from SD rats (8 weeks old, female, sterile). Briefly, ML were recovered and washed repeatedly in sterile saline to remove impurities. ML was placed in prewarmed serum-free RPMI 1640 medium containing 100 U/ml penicillin and 100 μg/mL streptomycin and incubated at 37°C and 5% CO2 for 24 h. Protein concentrations were determined using a BCA protein assay kit (GenStar, China) after the incubation was complete. Finally, ML-ES were collected and stored at −80°C until use.[56]

Cell culture and induction of differentiation

Mouse C2C12 myogenic cell lines were obtained from the American Type Culture Collection (ATCC, Manassas, VA) and cultured at 37°C in 5% CO2 in growth medium (GM) consisting of high-glucose Dulbecco's modified Eagle's medium (DMEM, Gibco, USA) supplemented with 10% (v/v) fetal bovine serum (FBS, Gibco, USA), 4 mM L-glutamine, 100 U/ml penicillin and 100 μg/mL streptomycin. Lentiviral transfection and screening were then performed after growth to the appropriate density. In the differentiation study, C2C12 muscle cells were grown in GM to reach 80% confluence and were then transferred to preheated differentiation medium (DM) consisting of DMEM containing 2% (v/w) heat-inactivated horse serum (HS, Gibco, USA), 4 mM glutamine, 100 U/ml penicillin and 100 μg/mL streptomycin.[11] Then, cell samples were collected at different periods of growth at the specified concentration. The cells were tested for mycoplasma contamination and found to be negative.

T. spiralis RNAi

T. spiralis and NBL were collected by digestion, washed with sterile PBS, and transferred to Opti-MEM. The diluted siRNA was mixed with 2 μL of X-treme GENE HP DNA transfection reagent (Roche, Germany) and incubated for 1 min. The diluted transfection reagent and newborn

larvae were mixed and incubated for 5 min at room temperature to form the transfection mixture. Transferred to the electric cup, and the following parameters were used for homeostatic clicking to introduce siRNA into the parasites: a voltage of 600 V, 25 μf, and 200 Ω (Gene Pulser type II, Bio-Rad). Afterward, the reactions were transferred to 24-well plates and supplemented with medium for incubation for 24 h at 37°C for follow-up experiments.

METHOD DETAILS

Transfection

Lentivirus transfection: The number of cells per well in the 6-well plate was approximately 2*105, and transfection was carried out when the cell density reached 60%–80%. The lentivirus supernatant was gently mixed and then added to C2C12 cells to be infected, and 5 μL of polybrene and 1 mL of DMEM containing 10% FBS were added and cultured at 37°C and 5% CO2. After 6 h of infection, the supernatant, which contained lentivirus and polybrene, was discarded, and 2 mL of medium (containing 10% serum) was added to each well for incubation at 37°C and 5% CO2. The same method was used to prepare the NC. The volume of added virus was calculated according to the following formula: MOI= (virus titer × virus volume)/number of cells. At MOI = 100, the Lv-*Ts*-RNF lentivirus titer was 1.21 * 10 ^ 9 TU/mL, and the Lv-NC and NC lentivirus titers were 2.91 * 10 ^ 9 TU/mL. On the third day of infection, DMEM containing 2.5 μg/mL puromycin and 10% FBS was used to replace the medium to screen the cells. According to the cell screening conditions, DMEM containing 2.5 μg/mL puromycin and 10% FBS was used to replace the medium every day. After 1 week, all the nonresistant cells died, the surviving cells were expanded and cultured in complete medium containing reducing puromycin, and a stable cell line was established.

293T cells were cultured in 6-well plates, and the number of cells in each well was approximately 2*105. When the cell density reached 70%–90%, the cells were transfected. Lipofectamine 2000 reagent and DNA were diluted in Opti-MEM. The diluted DNA was added to the diluted Lipofectamine 2000 reagent (1:1 ratio) and incubated for 5 min at room temperature. The DNA-lipid complexes were then added to the cells. The cells were incubated at 37°C and 5% CO2 for 1–3 days, and then the cells were collected.

Immunofluorescence analysis

On day 8 of C2C12 cell differentiation, the cover slides in 24-wells were cleaned with 0.01 M PBS, then fixed with precooled 4% (w/w) paraformaldehyde for 15 min, incubated with 0.1% Triton X-100 in PBS for 10 min, and sealed with 5% (v/w) goat serum in PBS for 2 h. Next, the cells were incubated overnight at 4°C with the primary antibodies anti-MyHC antibody, anti-SQSTM1/p62 antibody, and anti-tubulin antibody. Slides were washed with 0.01 M PBS three times and incubated with the secondary antibody goat anti-rabbit IgG Alexa Fluor 488 (ab150134, Abcam, UK) for 2 h at room temperature in the dark. For nuclear staining, cells were incubated with Hoechst 33342 at room temperature for 10 min, then washed with 0.01 M PBS three times. A cover glass was placed on the slide with 10 μL of anti-fading mounting solution (Beyotime, China). Finally, observed by laser confocal microscopy.

Quantitative proteomic analysis of ubiquitination

On day 8 of C2C12 cell differentiation (three biological replicates per group), TP + MG132 was added to 20 μM MG132 for 6 h, then cells were centrifuged at 16,000 × g for 15 min. Precipitate from each group was collected and stored at −80°C. Samples were removed from −80°C, lysed separately by adding 4× volume of lysis buffer (8 M urea, 1% protease inhibitor, 50 μM PR-619), sonicated at 4°C, and centrifuged at 12,000 × g for 10 min to remove debris. Supernatant was transferred to centrifuge tubes for protein concentration determination via BCA kit. After extraction, ubiquitin-modified proteomic and MS analyses were performed by PTM Biolabs (Hangzhou, China). Briefly, Proteins were resuspended and reduced, digested with trypsin, and desalted. The efficient enrichment of ubiquitinated peptides with diglycine remnant from digested peptide pools was accomplished by immunoprecipitation using anti-K-ε-GG antibody (PTM bio, Hangzhou, China). The resulted peptides were analyzed on Q Exactive HF Mass Spectrometer (Thermo). The identification and quantification of ubiquitinated peptides and proteins were done by MaxQuant. The tandem mass spectra were searched against UniProt mouse protein database together with a set of commonly observed contaminants. The FDR at peptide spectrum match level and protein level were controlled below 1%. The quantification of proteins was done by the module of label free quantification in MaxQuant.

Co-IP assays for analysis of protein–protein interactions

Cell samples were collected on day 8 of C2C12 cell differentiation (three biological replicates were used per group). The cells were lysed in lysis buffer (50 mM Tris–HCl pH 7.5, 150 mM NaCl, 1 mM EDTA, 0.5% Triton X-100, protease inhibitors (complete protease inhibitor cocktail tablets, Roche Diagnostics). Then, 200 μL of binding buffer was added to a 1-mL spin column. Using a wide-bore pipette tip, 50 μL settled resin slurry (25 μL settled resin) of Pierce DYKDDDDK Affinity Resin was placed into the column; the plug was removed and a spin column was inserted into a 2-mL collection tube. The column assembly was capped and centrifuged for 1 min at 1,000 × g. The liquid from the collection tube was discarded. The column was capped and 250 μL (10 bed volumes) of binding buffer was added. The column was capped and flicked to resuspend the resin. The plug was removed, and the column was inserted into the collection tube. The assembly was then centrifuged for 1 min at 1,000 × g. The resin was washed twice. The column was capped, and the prepared sample (300–800 μL) was added to the resin. The column was capped and resuspended by flicking or gentle vortexing. The column was placed on a rotator and mixed for 20 min at room temperature. The plug was removed and inserted into a clean collection tube, followed by centrifugation for 1 min at 1,000 × g. The flow-through fraction was saved for subsequent downstream analysis. The column was capped, and 250 μL (10-bed volumes) of wash buffer was added. The

column was again capped and flicked to resuspend the resin. The plug was removed, and the column was inserted into a collection tube, followed by centrifugation for 1 min at 1,000 × g and repeated washing for a total of two washes. The column was again capped, and 250 μL (10-bed volumes) of purified water was added. The column was again capped and flicked to resuspend the resin. The plug was then removed, and the column was inserted into the collection tube, followed by centrifugation for 1 min at 1,000 × g. The resin was transferred to a tube. Then, 100 μL of SDS-PAGE sample buffer was added to the tube. The sample was gently vortexed to mix the components and incubated at 95°C–100°C for 5–10 min. The resin was then centrifuged and removed, and the supernatant, containing the eluted target, was retained. Subsequently, Flag was detected by immunoblotting, and sequencing by MS was conducted.

Ubiquitination assays

To analyze the interaction of *Ts*-RNF with p62. HEK293T cells were cotransfected with Flag-*Ts*-RNF and the Myc-p62, △13–165, △187–297, △334–434 expression plasmids. Whole-cell extracts were then immunoprecipitated with anti-FLAG beads and analyzed by immunoblotting with anti-Myc antibodies. Next, we wanted to determine the specific sites of interaction between *Ts*-RNF and the p62.The Flag-*Ts*-RNF and Myc-p62, 422K/R and 437K/R expression plasmids were cotransfected into HEK293T cells, and co-IP experiments were performed by anti-FLAG beads followed by immunoblotting with anti-Myc antibodies. We next sought to determine the type of ubiquitin linkage on K422 of p62. HEK293T cells were transfected with Myc-p62, HA-Ub (WT) or HA-Ub mutants and Flag-*Ts*-RNF, and then whole-cell extracts were then immunoprecipitated with anti-Myc antibodies and analyzed by immunoblotting with anti-HA antibodies. For *in vitro* ubiquitination assay, *Ts*-RNF and P62 proteins were expressed *in vitro* with the TNT Quick Coupled Transcription/Translation Systems (Promega, USA) according to the manufacturer's protocol.[57] *In vitro* interaction and ubiquitination assays were performed as described (Boston Biochem, USA).[57]

Quantitative real-time PCR

Total RNA was extracted from C2C12 cells, HEK293T cells, and diaphragm samples using an RNAiso Plus (TaKaRa) kit according to the manufacturer's instructions. Total RNA mass and concentration were determined using a Nanodrop 2000 spectrophotometer (Thermo Fisher Scientific, USA). The RNA was then reverse transcribed into cDNA using One-Step gDNA Removal and cDNA Synthesis Super Mix (TransGen Biotech, China) as recommended by the supplier. The resulting cDNA was analyzed by qRT−PCR using an Applied Biosystems StepOne Plus Real-Time PCR system (Thermo Fisher Scientific, USA). Each sample was tested in duplicate in three wells on the same plate, and each reaction contained FastStart Essential DNA Green Master Mix (Roche, Germany), forward primer (0.2 μM), reverse primer (0.2 μM), and cDNA template. The reaction also contained 20 μL of nuclease-free water. All genes were amplified under the following conditions: incubation at 95°C for 5 min, followed by 40 cycles of denaturation at 95°C for 15 s and annealing at 60°C for 30 s. The relative CT ($2^{-\Delta\Delta Ct}$) method was used to analyze the mRNA expression levels.

Western blot analysis

Total proteins were extracted from cells and tissues, a mixture of protease inhibitor (Beyotime, China) was added, the protein concentration was determined using the BCA Protein Assay kit (Solarbio, China), and equal amounts of proteins were separated by 10% sodium dodecyl sulfate−polyacrylamide gel electrophoresis (SDS−PAGE). The separated bands were then transferred to a polyvinylidene difluoride (PVDF) membrane (Roche, Germany). The membranes were blocked in PBST containing 5% (w/v) skim milk for 2 h at room temperature, followed by incubation with primary antibodies overnight. Afterward, the membranes were washed five times with PBST and incubated with an HRP-linked anti-rabbit IgG antibody (#7074, Cell Signaling Technology, USA) in blocking buffer for 2 h at room temperature. Signals were detected using Pierce ECL western blotting substrate (Thermo Fisher Scientific, USA) and UVP Chemstudio (Analytik Jena, Germany) according to the manufacturer's instructions.

Mitochondrial membrane potential and superoxide anion assays

C2C12 cells differentiated for 8 days in a six-well plate were removed from the culture medium and washed with an appropriate volume of PBS. One milliliter of a working TMRE staining solution was added, and the cells were incubated in a cell incubator for 30 min at 37°C. After incubation, the supernatant was removed by aspiration, and the cells were washed twice with pre-warmed cell culture medium. Two milliliters of pre-heated cell culture medium were added, and the cells were observed under a fluorescence microscope. C2C12 cells differentiated for 8 days in six-well plates were aspirated from the culture medium and washed with an appropriate volume of PBS. Two hundred microliters of a working superoxide detection solution were added to each well, and the cells were incubated at 37°C for 3 min. Two microliters of an SOD solution were added to the NC sample to validate the assay, after which the absorbance at 450 nm was measured.

TEM

Skeletal muscle samples from infected mice were isolated on days 3, 10, and 17, rinsed with 7.5% sucrose buffer containing 0.1 M sodium octanoate, and then fixed in a buffered 0.1 M sodium octanoate and 2.5% glutaraldehyde solution at 4°C. Next, 1% osmium tetroxide (OsO4) in 0.033 M veronal acetate buffer containing 4% sucrose was added at 4°C for postfixation. The tissue samples were washed with 0.05 M veronal acetate buffer containing 6% sucrose and then treated with a 50% ethanol/EMbed 812 mixtures (1:1) for 2 h at room temperature, followed by treatment with a 100% ethanol/EMbed 812 mixtures (2:3) overnight. Subsequently, the tissue samples were treated with an EMbed 812 resin mixture without DMP-30 for 2 h at room temperature. The tissue was then transferred to gelatin capsules covered with an

EMbed 812 resin mixture containing DMP-30 and polymerized at 60°C for approximately 36 h. The sections were stained with 2% uranyl acetate in the dark for 15 min and then rinsed in ultrapure water. The cells were again stained with Raynaud's solution (pH 12.4) for 10 min and rinsed with 0.05 M NaOH Titrisol and CO_2-free ultrapure water. Finally, TEM was used at an accelerating voltage of 80 kV to observe the samples.

Ethics

Animals were treated according to the guidelines of the National Institute of Health (publication No. 85–23, revised 1996). Animal protocols were reviewed and approved by the Ethical Committee of Jilin University affiliated with the Provincial Animal Health Committee, Jilin Province, China (ethical clearance number IZ-2009-08).

QUANTIFICATION AND STATISTICAL ANALYSIS

Data are shown as the means ± SEMs from three independent experiments (GraphPad Prism software). Statistical analysis was performed by using Mann-Whitney U, independent sample t tests, and One-way ANOVA. Statistical significance is indicated as follows: *$p < 0.05$, **$p < 0.01$, ***$p < 0.001$, ns, not significant. Western blot data are representative, and the results from 3 independent experiments were similar.